

Alleviating the H_0 tension in Rastall gravity

R. Mohebi, Kh. Saaidi*, T. Golanbary† and K. Karami‡

Department of Physics, University of Kurdistan, P.O. Box 66177-15175, Sanandaj, Iran

(Dated: August 29, 2025)

Abstract

The tension between measurements of the Hubble constant H_0 locally and the value inferred from Planck satellite have provided a strong motivation to explore theoretical frameworks beyond the standard cosmological model (Λ CDM). To this aim, we investigate the H_0 tension in the Rastall Λ CDM model (R- Λ CDM), formulated within the Rastall gravity framework as a phenomenological extension of General Relativity featuring a non-conserved energy-momentum tensor. To constrain the cosmological parameters, we employ a comprehensive combined dataset including Big Bang Nucleosynthesis (BBN), Hubble parameter $H(z)$, Type Ia supernovae (SNe Ia), Baryon Acoustic Oscillations (BAO), Cosmic Microwave Background (CMB) anisotropies, and the growth rate of cosmic structures $f(z)\sigma_8(z)$. The estimation of model parameters is performed via Markov Chain Monte Carlo (MCMC) sampling within a Bayesian statistical framework. Our results show that the R- Λ CDM model, especially in closed geometry, reduces the H_0 tension, bringing the discrepancy with the local SH0ES measurements down to 1.97σ to 2.18σ . However, the tension related to the σ_8 parameter remains unresolved.

* ksaaidi@uok.ac.ir

† t.golanbary@uok.ac.ir

‡ kkarami@uok.ac.ir

I. INTRODUCTION

In modern cosmology, there are several significant topics of discussion, so that two of the most prominent being the tension in estimating the Hubble constant H_0 and the nature of dark energy. Understanding these issues can lead to new physics, motivating scientists to investigate them further. Various experiments have been conducted to explore the properties of dark energy and the accelerated expansion of the universe. Cosmologists have been striving to find an appropriate model to explain the late-time positive cosmic acceleration, leading to extensive research on gravitational theories [1–8].

Einstein’s general relativity (GR) with the inclusion of a cosmological constant remains the preferred theory of gravity for explaining the accelerated expansion of the universe. However, GR often encounters singularities and parameter degeneracies on cosmological scales. These drawbacks have prompted cosmologists to search for ways to overcome these issues. Inflationary cosmology is one of the modification which received huge acceptance by the scientists. Although the theory was proposed to solve the big bang problems, its predictions, such as quantum fluctuations, and its consistency with the observation made the theory as the cornerstone of any cosmological model [9–35]. Although inflation pertains to the earliest moments of cosmic history, its consequences extend to late-time observables, including implications for the current Hubble rate. To explain the observed cosmic acceleration, the cosmological constant and dark energy remain popular candidates. The dark energy model is one of the most well-known attempts to explain the late-time acceleration of the universe. On the other hand, cosmologists have explored various modified gravity theories, like $f(R)$ gravity [36–38], $f(T)$ gravity [39–41], $f(R, T)$ gravity [42–46], modified Gauss-Bonnet gravity $f(G)$ [47–49], scalar-tensor gravity [50–52], brane gravity [53–55] and so on. One of another theories is Rastall Gravity [56–59], which arises from a constraint on the energy-momentum tensor. In general, modified gravitational theories extend the Einstein-Hilbert action of General Relativity using the curvature description of gravity.

Among the various outstanding issues in modern cosmology, the tension in the measurements of the Hubble constant H_0 remains one of the most significant and persistent challenges in modern cosmology. In recent years, this discrepancy has become increasingly prominent due to the divergence between two independent measurement techniques. The Planck collaboration, based on seven years of observations and analysis of the cosmic microwave background (CMB), has reported a value of $H_0 = 67.4 \pm 0.5 \text{ km s}^{-1} \text{ Mpc}^{-1}$ [60–62]. In contrast, the SH0ES (Supernovae H_0 for the Equation of State) team, utilizing distance ladder measurements with the Hubble Space Telescope (HST), has obtained a significantly higher value of $H_0 = 73.2 \pm 1.3 \text{ km s}^{-1} \text{ Mpc}^{-1}$. This discrepancy, often referred to as the “Hubble tension”, has profound implications for our understanding of the universe’s expansion history and may point to new physics beyond the standard cosmological model [63–65].

The HST method involves measurements of the local distance ladder by combining photometry from Cepheids (and their period-luminosity relation) with other local distance anchors, such as Milky Way parallaxes and calibration distances to Cepheids in nearby galaxies that host SNe Ia. Specifically, for estimating the Hubble constant, the observations of 70 Cepheids in the Large Magellanic Cloud are used by the HST group [64]. Currently, the discrepancy between H_0 estimations by the Hubble Space Telescope (HST) [61] and the Planck [61] collaboration exceeds 4σ . This tension has persisted over the years, as shown in Table I. The problem can be seen as a discrepancy between early and late cosmological observations of our Universe. The HST group uses late-time data, while the Planck collaboration combines observations from redshifts in a wide range ($0 < z < 1100$) using the standard Λ CDM model as the fiducial model.

Different methods have been proposed to address the H_0 tension. Various groups have analyzed H_0 estimations using methods independent of the Cepheid distance scale and CMB anisotropies [66, 67]. Among these methods, the following approaches have provided noteworthy results for H_0 :

- Lensing objects with strong time delays between multiple images (H0LiCOW project and others) [68, 69].
- CMB-lensing data [68].
- The tip of the red giant branch (TRGB) method used by the Carnegie-Chicago Hubble Program (CCHP) [70, 71].
- Maser (megamaser) hosting galaxies [72].
- Oxygen-rich variable stars (Miras) [73].

Some researchers have also suggested that the Planck or HST measurements might suffer from systematic errors, but these analyses have not provided convincing solutions to the problem.

As shown in Table I, the value of the Hubble constant H_0 varies between the Planck 2018 result [60] and the SH0ES 2021 measurement of $H_0 = 73.2 \pm 1.3 \text{ km s}^{-1} \text{ Mpc}^{-1}$ [64]. The recent measurements of H_0 are in better agreement

TABLE I: Estimations of H_0 ($\text{km s}^{-1} \text{Mpc}^{-1}$) from different observational methods.

H_0	Project	Method	Year	Ref.
67.4 ± 0.5	Planck	CMB Power Spectra-Lensing	2018	[60]
73.2 ± 1.3	SH0ES (HST)	Cepheid distance ladder	2019	[64]
72.7 ± 4.6	HST	6 Miras in SN Ia host galaxy	2019	[74]
$73.3^{+1.7}_{-1.8}$	HoLiCOW	6 strong lenses and Λ CDM	2019	[68]
$69.6^{+0.8}_{-1.7}$	CCHP	TRGB	2020	[71]
73.9 ± 3.0	6 maser galaxies	Megamaser	2020	[73]
68.0 ± 0.36	ACT DR6	CMB Power Spectra (TT, TE, EE)	2025	[75]
71.0 ± 1.1	ACT DR6 + DESI DR2	CMB + BAO + EDE model fit	2025	[76]

with the late-universe results from the Hubble Space Telescope (SH0ES 2021), showing a notable divergence from the early-universe values obtained by the Planck collaboration.

In light of this tension in H_0 measurements, cosmologists have explored various extensions to the standard cosmological model that may account for the discrepancy. To address this issue, several theoretical scenarios have been proposed, including modified gravity theories [77–79], alternative dark energy models [80], frameworks involving extra relativistic species [81], and models with interactions between dark energy and dark matter [82].

In this paper, we conduct a detailed investigation of the persistent tension in the measurement of the Hubble constant H_0 , which remains one of the most significant and unresolved challenges in modern cosmology. This tension refers to the statistically significant discrepancy between the value of H_0 obtained from early-Universe probes such as the Cosmic Microwave Background (CMB) and the value derived from late-Universe measurements, including Type Ia supernovae and local distance ladder methods. Such a discrepancy may indicate possible deviations from the Λ CDM model or the presence of new fundamental physics.

To address this issue, we consider the energy-momentum tensor incorporating various components such as cold dark matter, radiation, and dark energy within the framework of Rastall gravity, a phenomenological modification of general relativity in which the usual conservation laws of energy-momentum are slightly altered. By applying the Rastall hypothesis in the cosmological context, we develop and analyze models that allow for an effective interaction between matter fields and spacetime geometry, potentially leading to nontrivial modifications in the dynamics of cosmic expansion. Our goal is to systematically examine how these modifications affect cosmic evolution and whether the altered gravitational dynamics can naturally alleviate the H_0 tension. This approach not only offers a novel theoretical perspective but also provides the possibility of constraining parameters of modified gravity through cosmological observations.

This paper is organized as follows. In Section II, we provide an overview of the cosmological models and parameters considered in this study. The observational data are described in Section III. Section IV outlines the methodology used for model evaluation and parameter estimation. The results, including constraints on the cosmological parameters and their implications for the H_0 tension, are presented in Section V. Finally, Section VI summarizes the main findings and discusses potential directions for future work. For completeness, Appendix A provides the statistical estimator used to quantify the tension between datasets.

II. COSMOLOGICAL MODELS

To determine the Hubble parameter $H(z)$ in different cosmological models, we begin with Einstein’s field equations in general relativity

$$R_{\mu\nu} - \frac{1}{2}Rg_{\mu\nu} = 8\pi GT_{\mu\nu}, \quad (1)$$

where $g_{\mu\nu}$ is the metric tensor, G is Newton’s gravitational constant, and for simplicity we set $8\pi G = 1$. The tensors $R_{\mu\nu}$ and R denote the Ricci tensor and Ricci scalar, respectively. The energy-momentum tensor $T_{\mu\nu}$ describes the total energy content of the universe, including matter, radiation, and dark energy, and is defined as

$$T_{\mu\nu} = \sum_i T_{\mu\nu}^i,$$

where the index i labels the individual components: baryonic and cold dark matter ($i = m$), radiation ($i = r$), and dark energy ($i = \Lambda$). Each component is modeled as a perfect fluid, characterized by the energy-momentum tensor

$$T_i^{\mu\nu} = (\rho_i + p_i)u^\mu u^\nu + p_i g^{\mu\nu}, \quad (2)$$

where ρ_i and p_i are the energy density and pressure of the i -th fluid, and u^μ is the four-velocity. The conservation of energy-momentum, $T_{\nu;\mu}^\mu = 0$, is compatible with the Bianchi identities, $G_{\nu;\mu}^\mu = 0$ [83].

Assuming spatial homogeneity and isotropy, the Einstein equations in a non-flat geometry reduce to the Friedmann equations

$$H^2 + \frac{k}{a^2} = \frac{1}{3} \sum_i \rho_i, \quad (3)$$

$$\frac{\ddot{a}}{a} = -\frac{1}{6} \sum_i (\rho_i + 3p_i). \quad (4)$$

The Hubble parameter is defined as $H \equiv \dot{a}/a$, where $a(t)$ is the cosmological scale factor and the overdot denotes differentiation with respect to cosmic time. The energy density associated with spatial curvature is given by $\rho_k = -3k/a^2$, where $k = 0, +1$, and -1 correspond to flat, closed, and open universes, respectively.

The evolution of each fluid component is determined by its equation of state, given by $p_i = \omega_i \rho_i$, where ω_i is the equation of state (EoS) parameter. For pressureless matter and cold dark matter, $\omega_m = 0$; for radiation, $\omega_r = 1/3$; for a cosmological constant, $\omega_\Lambda = -1$; and for a generic dark energy component X , one has $\omega_X < -1/3$.

In addition, the energy conservation equation is given by

$$\dot{\rho}_i = -3H(p_i + \rho_i) = -3H(1 + \omega_i)\rho_i. \quad (5)$$

Assuming a constant EoS parameter ω_i , the solution to Eq. (5) is

$$\rho_i(t) = \rho_0 \left(\frac{a_0}{a} \right)^{3(1+\omega_i)}, \quad (6)$$

where ρ_0 and a_0 denote the present values of the energy density and scale factor, respectively.

The dimensionless energy density parameters at present time are defined as

$$\Omega_{m_0} \equiv \frac{\rho_{m_0}}{3H_0^2}, \quad \Omega_{\Lambda_0} \equiv \frac{\Lambda}{3H_0^2}, \quad \Omega_{r_0} \equiv \frac{\rho_{r_0}}{3H_0^2}, \quad \Omega_{k_0} \equiv -\frac{k}{a_0^2 H_0^2}. \quad (7)$$

Using these definitions, the Friedmann equation (3) for the Λ CDM model can be written as

$$E(z; \mathbf{p}) \equiv \frac{H(z; \mathbf{p})}{H_0} = \left[\Omega_{m_0}(1+z)^3 + \Omega_{r_0}(1+z)^4 + \Omega_{k_0}(1+z)^2 + \Omega_{\Lambda_0} \right]^{1/2} \quad (8)$$

where $z = (a_0/a) - 1$ is the redshift, H_0 is the present Hubble parameter, and \mathbf{p} denotes the set of model parameters. The density parameter of the cosmological constant satisfies the closure condition $\Omega_{\Lambda_0} + \Omega_{m_0} + \Omega_{r_0} + \Omega_{k_0} = 1$.

A. Rastall Model

A notable approach to modifying general relativity involves introducing an explicit non-minimal coupling between geometry and matter. This coupling leads to a non-conservation of the energy-momentum tensor, resulting in a departure from geodesic motion and the appearance of an additional force [84]. Within this framework, Rastall proposed a modification to the Einstein field equations by relaxing the usual conservation condition for the matter energy-momentum tensor.

The aim here is to place constraints on cosmological parameters in both Λ CDM and its generalized counterpart, referred to as the R- Λ CDM model, in order to investigate their effectiveness in alleviating the H_0 tension. In Rastall gravity, the modified Einstein field equation is given by

$$G_{\mu\nu} = \kappa(T_{\mu\nu} + \hat{T}_{\mu\nu}), \quad (9)$$

where the additional tensor is given by $\hat{T}_{\mu\nu} = -\epsilon R g_{\mu\nu}$, and ϵ denotes the Rastall parameter. The gravitational coupling constant κ is expressed as

$$\kappa = 8\pi G \left(\frac{1 - 4\epsilon\kappa}{1 - 6\epsilon\kappa} \right). \quad (10)$$

By adopting the convention $8\pi G = 1$, the above relation reduces to the quadratic equation

$$12\epsilon^2\kappa^2 + \kappa(2\epsilon - 1) + 1 = 0. \quad (11)$$

The real solution for κ exist only if the Rastall parameter lies within the interval

$$\epsilon \in [-0.20, 0.11]. \quad (12)$$

In what follows, small deviations from general relativity are considered by restricting to the limit $|\epsilon\kappa| \ll 1$, which implies $\epsilon \in [-0.20, 0.11]$. Under this assumption, a perturbative expansion of Eq. (11) yields $\kappa \simeq 1 + 2\epsilon$. Substituting this into Eq. (9) gives the following approximate field equation

$$G_{\mu\nu} = T_{\mu\nu} + \epsilon [2T_{\mu\nu} - (1 + 2\epsilon)Rg_{\mu\nu}]. \quad (13)$$

Taking the trace of above equation results in

$$R = -(1 + 2\epsilon)(1 + 4\epsilon + 24\epsilon^2 + \dots)T. \quad (14)$$

Replacing this into Eq. (13) leads to the relation

$$G^\mu_\nu = T^\mu_\nu + \epsilon [2T^\mu_\nu + (1 + 8\epsilon)g^\mu_\nu T]. \quad (15)$$

To model the matter content of the universe, a perfect fluid is considered with energy-momentum tensor $T_{(i)\nu}^\mu = \text{diag}(-\rho_i, p_i, p_i, p_i)$, where the index i labels the individual components characterized by a constant EoS parameter $\omega_i \equiv p_i/\rho_i$. The four-velocity vector in the comoving frame is $u^\mu = (1, 0, 0, 0)$, satisfying $u_\mu u^\mu = -1$. In a non-flat universe, the corresponding modified Friedmann equation takes the form

$$H^2 + \frac{k}{a^2} = \frac{1}{3} \sum_i \rho_i [1 + 3\epsilon(1 - \omega_i) + 8\epsilon^2(1 - 3\omega_i)]. \quad (16)$$

In Rastall gravity, the energy conservation equation is given by

$$\dot{\rho}_i = -3\frac{\dot{a}}{a} \left[\frac{(1 + \omega_i)}{1 + \epsilon(1 + 6\epsilon)(3\omega_i - 1)} \right] \rho_i, \quad (17)$$

and its solution takes the form

$$\rho_i = \rho_0 \left(\frac{a_0}{a} \right)^{\left[\frac{3(1+\omega_i)}{1+\epsilon(1+6\epsilon)(3\omega_i-1)} \right]}. \quad (18)$$

To simplify the notation, a rescaled energy density parameter is introduced as

$$\tilde{\Omega}_i = \Omega_i [1 + 3\epsilon(1 - \omega_i) + 8\epsilon^2(1 - 3\omega_i)], \quad (19)$$

which allows the Friedmann equation to be expressed as

$$\begin{aligned} \frac{H(z; \mathbf{p})}{H_0} = & \left[\tilde{\Omega}_{m_0}(1+z)^{\frac{3}{1-\epsilon(1+6\epsilon)}} + \tilde{\Omega}_{r_0}(1+z)^4 \right. \\ & \left. + \Omega_{k_0}(1+z)^2 + \tilde{\Omega}_{\Lambda_0} \right]^{1/2} \end{aligned} \quad (20)$$

where

$$\tilde{\Omega}_{m_0} \equiv \Omega_{m_0} (1 + 3\epsilon + 8\epsilon^2), \quad (21)$$

$$\tilde{\Omega}_{r_0} \equiv \Omega_{r_0} (1 + 2\epsilon), \quad (22)$$

$$\tilde{\Omega}_{\Lambda_0} \equiv \Omega_{\Lambda_0} (1 + 6\epsilon + 32\epsilon^2), \quad (23)$$

and the closure relation implies $\tilde{\Omega}_{\Lambda_0} + \tilde{\Omega}_{m_0} + \tilde{\Omega}_{r_0} + \Omega_{k_0} = 1$.

III. OBSERVATIONAL DATA ANALYSIS

In the following, we aim to derive constraints on the parameters of both the standard and Rastall versions of the Λ CDM model. To this end, we apply the MCMC method to maximize the likelihood function $L(\mathbf{p})$, or equivalently minimize $\chi^2(\mathbf{p})$ [85], with respect to the parameter vector \mathbf{p} , in order to determine the best-fit values \mathbf{p}_0 . Confidence intervals at the 1σ , 2σ , and 3σ levels are defined as two-dimensional parameter contours.

For the calculation of $\chi^2(\mathbf{p})$, we use the following observational datasets

- BBN data, with one data point from [86],
- $H(z)$ data, incorporating 37 measurements as listed in Table II [85],
- Type Ia Supernovae data, specifically the 1048 Pantheon (SNP) measurements from [87],
- CMB data, with one point from [88],
- BAO data, including the three measurements from Tables I and II in [87],
- $f(z)\sigma_8(z)$ data points as listed in Table III [89].

Since the total likelihood is given by

$$L_{\text{tot}}(\mathbf{p}) = L_{\text{BBN}} \times L_{\text{H}} \times L_{\text{SN}} \times L_{\text{CMB}} \times L_{\text{BAO}} \times L_{f\sigma_8}, \quad (24)$$

the combined chi-square is

$$\begin{aligned} \chi_{\text{tot}}^2(\mathbf{p}) = & \chi_{\text{BBN}}^2(\mathbf{p}) + \chi_{\text{H}}^2(\mathbf{p}) + \chi_{\text{SN}}^2(\mathbf{p}) + \chi_{\text{CMB}}^2(\mathbf{p}) \\ & + \chi_{\text{BAO}}^2(\mathbf{p}) + \chi_{f\sigma_8}^2(\mathbf{p}). \end{aligned} \quad (25)$$

Finally, we employ the MCMC technique [90] to constrain the parameter vector \mathbf{p} within the frameworks of both the Λ CDM and R- Λ CDM.

A. Big Bang Nucleosynthesis (BBN data)

One of the primary elements commonly used to constrain the baryon density is the abundance of deuterium. In particular, the reaction involving the capture of a proton by deuterium to produce helium-3 plays an important role. The experimental value for the reaction rate is calculated in [91], which constrains the baryon density to $\Omega_{b_0} h^2 = 0.022 \pm 0.002$. The chi-square term χ_{BBN}^2 is given by

$$\chi_{\text{BBN}}^2(\mathbf{p}) = \frac{[\Omega_{b_0} h^2 - 0.022]^2}{(0.002)^2}. \quad (26)$$

B. Hubble parameter measurements ($H(z)$ data)

We use 37 independent $H(z)$ data points, listed in [85] and summarized in Table II, spanning a redshift range of $0.07 \leq z \leq 2.36$, to constrain the parameters of the cosmological models. The observational data include measurements of the Hubble parameter, $H_{\text{obs}}(z_i)$, at redshifts z_i , along with the corresponding 1σ uncertainties, σ_i . To constrain the cosmological parameters \mathbf{p} of the models, we compute the chi-squared statistic χ_{H}^2 as

$$\chi_{\text{H}}^2(H_0, \mathbf{p}) = \sum_{i=1}^{37} \frac{[H_{\text{th}}(z_i; H_0, \mathbf{p}) - H_{\text{obs}}(z_i)]^2}{\sigma_i^2}, \quad (27)$$

where $H_{\text{th}}(z_i; H_0, \mathbf{p})$ denotes the theoretical prediction of the Hubble parameter at redshift z_i for a given model.

TABLE II: The Hubble parameter data (in $\text{km s}^{-1} \text{Mpc}^{-1}$) versus redshift [85].

z	$H(z)$	σ_H	Ref.	z	$H(z)$	σ_H	Ref.
0.0708	69	19.68	[92]	0.6	87.9	6.1	[93]
0.09	69	12	[94]	0.68	92	8	[95]
0.12	68.6	26.2	[92]	0.73	97.3	7	[96]
0.17	83	8	[94]	0.781	105	12	[93]
0.179	75	4	[96]	0.875	125	17	[96]
0.199	75	5	[96]	0.88	90	40	[96]
0.2	72.9	29.6	[92]	0.9	117	23	[97]
0.24	79.69	2.65	[94]	1.037	154	20	[94]
0.27	77	14	[92]	1.3	168	17	[96]
0.28	88.8	36.6	[96]	1.363	160	33.6	[94]
0.3	81.7	6.2	[95]	1.43	177	18	[98]
0.35	82.1	4.8	[99]	1.53	140	14	[94]
0.35	84.4	7	[94]	1.75	202	40	[94]
0.352	83	14	[99]	1.965	186.5	50.4	[94]
0.4	95	17	[93]	2.3	224	8	[98]
0.43	86.45	3.68	[99]	2.34	222	7	[100]
0.44	82.6	7.8	[97]	2.36	226	8	[101]
0.48	97	62	[95]				
0.57	89.2	3.6	[96]				
0.593	104	13	[95]				

C. Type Ia supernovae from the Pantheon compilation (SNe Ia data)

Standard candles, particularly Type Ia supernovae, serve as crucial cosmological probes due to their well-understood intrinsic luminosities, which allow for the measurement of relative distances. The distance modulus, $\mu(z)$, is theoretically related to the luminosity distance, $d_L(z)$, via

$$\mu(z) = 5 \log_{10} \left[\frac{d_L(z)}{10 \text{ pc}} \right]. \quad (28)$$

The chi-squared statistic for supernova observations is given by

$$\chi_{\text{SN}}^2 = \sum_i \frac{[\mu_{\text{th}}(z_i) - \mu_{\text{obs}}(z_i)]^2}{\sigma_i^2}. \quad (29)$$

The theoretical prediction for the distance modulus is formulated as

$$\mu_{\text{th}}(z) = 5 \log_{10} [(1+z)y(z)] + \mu_0, \quad (30)$$

where

$$\mu_0 = 42.384 - 5 \log_{10}(h), \quad (31)$$

and $h = H_0/100$ is the Hubble constant. Also, $y(z)$ is the dimensionless comoving distance defined as

$$y(z) = \begin{cases} \frac{1}{\sqrt{\Omega_{k_0}}} \sinh \left(\sqrt{\Omega_{k_0}} \int_0^z \frac{dz'}{E(z')} \right), & \text{for } \Omega_{k_0} > 0, \\ \int_0^z \frac{dz'}{E(z')}, & \text{for } \Omega_{k_0} = 0, \\ \frac{1}{\sqrt{-\Omega_{k_0}}} \sin \left(\sqrt{-\Omega_{k_0}} \int_0^z \frac{dz'}{E(z')} \right), & \text{for } \Omega_{k_0} < 0. \end{cases} \quad (32)$$

D. Cosmic Microwave Background (CMB data)

One of the most useful datasets for determining cosmological parameters is the location of the Cosmic Microwave Background (CMB) acoustic peaks. The location of these peaks is determined by the parameters (R, l_a, z_*) , where R is the scale distance to recombination, given by [102]

$$R = \sqrt{\Omega_{m_0}} H_0 r(z_*), \quad (33)$$

where $r(z)$ represents the comoving sound horizon distance defined as

$$r(z) = (1+z)D_A(z), \quad (34)$$

and $D_A(z)$ is the angular diameter distance expressed as

$$D_A(z) = \frac{y(z)}{H_0(1+z)}. \quad (35)$$

Also $y(z)$ is defined in Equation (32). Additionally, l_a is given by

$$l_a = \pi \frac{r(z_*)}{r_s(z_*)}, \quad (36)$$

where $r(z_*)$ is the comoving distance and $r_s(z_*)$ is the comoving sound horizon distance at the recombination point. This distance is defined by the following integral

$$r_s(a) = \int_0^a \frac{C_s(a') da'}{a'^2 H(a')}, \quad (37)$$

where $C_s(a')$ is the baryon sound speed, which is given by

$$C_s(a) = \frac{1}{\sqrt{3 \left(1 + a \frac{3\Omega_{b0}}{4\Omega_{r0}} \right)}}. \quad (38)$$

The radiation density parameter Ω_{r0} , which includes both photon and neutrino contributions, is now computed through cosmological data fitting in Sec. V. The last scattering epoch, or recombination redshift, z_* , is a weak function of parameters and is given by [103]

$$z_* = 1048 \left[1 + 0.00127(\Omega_{b0} h^2)^{-0.738} \right] \left[1 + g_1(\Omega_{b0} h^2)^{g_2} \right], \quad (39)$$

where

$$g_1 = \left[0.0783(\Omega_{b0} h^2)^{-0.238} \right] \left[1 + 39.5(\Omega_{b0} h^2)^{0.763} \right]^{-1}, \quad (40)$$

$$g_2 = 0.560 \left[1 + 21.1(\Omega_{b0} h^2)^{1.81} \right]^{-1}. \quad (41)$$

Finally, the chi-squared statistic χ_{CMB}^2 reads

$$\chi_{\text{CMB}}^2 = X_{\text{CMB}}^T C_{\text{CMB}}^{-1} X_{\text{CMB}}, \quad (42)$$

in which,

$$X_{\text{CMB}} = \begin{pmatrix} R - 1.7429 \\ l_a - 301.49 \\ \Omega_{b0} h^2 - 0.02260 \end{pmatrix}, \quad (43)$$

$$C_{\text{CMB}}^{-1} = \begin{pmatrix} 102243 & -1565.42 & 1.94853 \times 10^6 \\ -1565.42 & 170.59 & 3130.83 \\ 1.94853 \times 10^6 & 3130.83 & 7.91479 \times 10^7 \end{pmatrix}. \quad (44)$$

E. Baryon Acoustic Oscillations (BAO data)

Another dataset considered in this work is the BAO sample. We divide this datasets into two groups, as organized in Tables II and III of [87]. In the first case, the theoretical prediction is given by [87]

$$d_{\text{th}}(z) = \frac{r_s(z_d)}{D_v(z)}. \quad (45)$$

Here, $D_v(z)$ is the effective distance ratio, and z_d is the redshift of the drag epoch, which depends more strongly on cosmological parameters. These are defined as [103]

$$D_v(z) = \left[(1+z)^2 D_A^2(z) \frac{z}{H(z)} \right]^{1/3}, \quad (46)$$

$$z_d = 1345 \frac{(\Omega_{b_0} h^2)^{0.251}}{1 + 0.659(\Omega_{b_0} h^2)^{0.828}} [1 + b_1(\Omega_{b_0} h^2)^{b_2}], \quad (47)$$

and

$$\begin{aligned} b_1 &= 0.313(\Omega_{b_0} h^2)^{-0.419} [1 + 0.607(\Omega_{b_0} h^2)^{0.674}], \\ b_2 &= 0.238(\Omega_{b_0} h^2)^{0.223} \end{aligned}$$

The corresponding chi-squared function for the first case is

$$\chi_{\text{BAO},1}^2 = \sum_i \frac{[d_{z,i} - d_z(z_i)]^2}{\sigma_i^2}. \quad (48)$$

In the second case, the corresponding chi-squared function is

$$\chi_{\text{BAO},2}^2 = [\alpha_i^* - \alpha^*(z_i)] \cdot \Sigma_{\text{BAO},ij}^{-1} \cdot [\alpha_j^* - \alpha^*(z_j)], \quad (49)$$

where

$$\alpha^*(z) = \frac{D_v(z)}{r_s(z_d)} r_s^{\text{fid}}. \quad (50)$$

The data points are assumed to be uncorrelated, except for the WiggleZ subset listed in Table III of [87], whose covariance matrix is given by

$$\Sigma_{\text{WiggleZ}} = \begin{pmatrix} 6889 & -8961 & 21277 \\ -8961 & 10201 & -13918 \\ 21277 & -13918 & 7396 \end{pmatrix}. \quad (51)$$

The WiggleZ data at three redshifts ($z = 0.44, 0.6$, and 0.73) are reported in Table III of [87].

F. The growth rate of cosmic structures ($f(z)\sigma_8(z)$ data)

The geometrical data introduced in the previous sections are all related to the expansion history of the universe. One of the most important topics in modern cosmology is the study of the formation of large-scale structures using observational data related to the growth of cosmic inhomogeneities.

In this work, we use 18 independent $f(z)\sigma_8(z)$ data points as compiled in [89]. Due to the statistical independence of these measurements, the chi-squared function can be written as

$$\chi_{f\sigma_8}^2 = \sum_i \frac{[f\sigma_{8,\text{th}}(z_i) - f\sigma_{8,\text{obs}}(z_i)]^2}{\sigma_i^2}. \quad (52)$$

According to the cosmological principle, the universe is homogeneous and isotropic on scales larger than 100 Mpc. However, data from the COBE and WMAP satellites confirm that the CMB exhibits temperature anisotropies of the

TABLE III: The observational function $f(z)\sigma_8(z)$ versus redshift [89].

z	$f(z)\sigma_8(z)$	σ	Ref.
0.02	0.428	0.0465	[104]
0.02	0.398	0.065	[105, 106]
0.02	0.314	0.048	[105, 107]
0.10	0.370	0.130	[108]
0.15	0.490	0.145	[109]
0.17	0.510	0.060	[110]
0.18	0.360	0.090	[111]
0.38	0.440	0.060	[111]
0.25	0.3512	0.0583	[112]
0.37	0.4602	0.0378	[112]
0.32	0.384	0.095	[113]
0.59	0.488	0.060	[114]
0.44	0.413	0.080	[93]
0.60	0.390	0.063	[93]
0.73	0.437	0.072	[93]
0.60	0.550	0.120	[115]
0.86	0.400	0.110	[115]
1.40	0.482	0.116	[116]

order $\Delta T/T \sim 10^{-5}$. These temperature fluctuations reflect primordial density fluctuations. Such inhomogeneities grow during the matter-dominated era due to gravitational instability and eventually lead to the large-scale structures we observe today. The formation of today's nonlinear structures, such as galaxies and galaxy clusters, from initial small perturbations is a direct consequence of the theory of gravitational instability.

To study this, we consider an element of the universe with energy density $\epsilon(\vec{r}, t)$. At a given time t , the spatial average energy density is

$$\bar{\epsilon}(t) = \frac{1}{V} \int_V \epsilon(\vec{r}, t) d^3r. \quad (53)$$

To quantify the local deviations from the mean density, we define the density contrast as

$$\delta(\vec{r}, t) \equiv \frac{\epsilon(\vec{r}, t) - \bar{\epsilon}(t)}{\bar{\epsilon}(t)}. \quad (54)$$

In the linear regime, small perturbations ($\delta \ll 1$) grow under the influence of gravity. Using relativistic perturbation theory, one arrives at the following coupled differential equations [117]:

$$\delta_m'' + A_m \delta_m' + B_m \delta_m = \frac{3}{2a^2} [\Omega_m \delta_m + (1 + 3C_{\text{eff}}^2) \Omega_\Lambda \delta_\Lambda], \quad (55)$$

$$\delta_\Lambda'' + A_\Lambda \delta_\Lambda' + B_\Lambda \delta_\Lambda = \frac{3}{2a^2} (1 + \omega_\Lambda) [\Omega_m \delta_m + (1 + 3C_{\text{eff}}^2) \Omega_\Lambda \delta_\Lambda], \quad (56)$$

where the prime symbol denotes differentiation with respect to the scale factor a . The coefficients appearing in these equations are given by:

$$\begin{aligned} A_m &= \frac{3}{2a} (1 - w_\Lambda \Omega_\Lambda), \\ B_m &= 0, \\ A_\Lambda &= \frac{1}{a} \left[-3w_\Lambda - \frac{aw'_\Lambda}{1 + w_\Lambda} + \frac{3}{2} (1 - w_\Lambda \Omega_\Lambda) \right], \\ B_\Lambda &= \frac{1}{a^2} \left[-aw'_\Lambda + \frac{aw'_\Lambda w_\Lambda}{1 + w_\Lambda} - \frac{1}{2} w_\Lambda (1 - 3w_\Lambda \Omega_\Lambda) \right]. \end{aligned}$$

In this work, we consider the case of homogeneous dark energy, assuming an effective squared sound speed $C_{\text{eff}}^2 = 1$ and vanishing perturbations, $\delta_\Lambda = 0$. This assumption is well justified, as dark energy perturbations are suppressed on sub-horizon scales and do not grow via gravitational instability [102].

The growth rate function $f(z)$ and the matter fluctuation amplitude $\sigma_8(z)$ are defined as:

$$f(z) = \frac{d \ln \delta_m}{d \ln a} = \frac{\delta'_m(a)}{a \delta_m(a)}, \quad (57)$$

$$\sigma_8(z) = \sigma_8(z=0) \frac{\delta_m(z)}{\delta_m(z=0)}. \quad (58)$$

The product $f(z)\sigma_8(z)$ is a directly measurable quantity and serves as a key observational probe for testing cosmological models.

IV. CONSTRAINTS ON MODELS

In this section, we employ the MCMC technique to derive the best-fit values of the model parameters. The analysis is performed using a comprehensive dataset that includes BBN, $H(z)$, BAO, SNe Ia, CMB and $f\sigma_8(z)$ observations.

Both the standard Λ CDM and R- Λ CDM models are investigated under the assumptions of spatially flat and non-flat universes. The results of the parameter fitting are summarized in Tables IV to XII, and the corresponding confidence contours are illustrated in Figures 1 to 6.

To assess the sensitivity of our constraints to different combinations of data, we define the following datasets

- $D_1 = \text{BBN} + \text{H} + \text{BAO} + \text{SN} + \text{CMB} + f\sigma_8$
- $D_2 = \text{BBN} + \text{H} + \text{BAO} + \text{SN} + f\sigma_8$
- $D_3 = \text{BBN} + \text{H} + \text{BAO} + \text{SN} + \text{CMB}$
- $D_4 = \text{Table 2 of [60]}$ (includes TT, TE, EE+lowE+lensing+BAO datasets)

where H refers $H(z)$ data. Model selection is carried out using the AIC and the BIC, which are widely used statistical tools for model comparison [118–123]. The expressions for AIC and BIC are given by

$$\text{AIC} = \chi^2_{\min} + 2d, \quad (59)$$

$$\text{BIC} = \chi^2_{\min} + d \ln N, \quad (60)$$

where d is the number of model parameters and N is the total number of observational data points. According to the ΔAIC criterion, a difference of $\Delta\text{AIC} \leq 2$ implies substantial support for the model. Values in the range $4 \leq \Delta\text{AIC} \leq 7$ indicate considerably less support, while $\Delta\text{AIC} \geq 10$ suggests that the model is strongly disfavored [121]. Similarly, in the context of the BIC, a value of $\Delta\text{BIC} \leq 2$ is regarded as weak evidence, $2 \leq \Delta\text{BIC} \leq 6$ indicates positive evidence, $6 \leq \Delta\text{BIC} \leq 10$ reflects strong evidence, and values exceeding 10 are interpreted as very strong evidence against the model with the higher BIC [119].

V. NUMERICAL RESULTS

A. Constraining the flat and non-flat models of Λ CDM

Here, we analyze both flat and non-flat Λ CDM cosmological models by employing various combinations of the observational datasets introduced earlier. We report the resulting constraints on the cosmological parameters, together with the corresponding goodness-of-fit statistics and an assessment of the internal consistency across different data combinations. Furthermore, to quantify possible discrepancies between datasets, we utilize a statistical estimator to evaluate the level of tension in the inferred parameters (see Appendix A). Finally, we provide an updated summary of parameter estimations within the Λ CDM framework.

1. Flat Λ CDM model

We perform a comprehensive comparison of the datasets D_1 , D_2 , D_3 , and D_4 within the framework of the flat Λ CDM model. The constraints on the cosmological parameters of the six-parameter flat Λ CDM model derived from these datasets are summarized in Table IV and illustrated in Figure 1. This table reports the 68% confidence intervals for the cosmological parameters derived from datasets D_1 , D_2 , D_3 , and D_4 . The estimated Hubble constant values, H_0 , lie within the range of approximately 67.2 to 69.0 km s⁻¹ Mpc⁻¹, reflecting the current expansion rate of the universe. In particular, the H_0 value obtained from dataset D_2 , which does not include CMB data, is 69.0 ± 1.2 km s⁻¹ Mpc⁻¹. This estimate deviates from the Planck 2018 value of 67.4 ± 0.5 km s⁻¹ Mpc⁻¹ by about 1.23σ , while it is only 2.37σ away from the local measurement reported by SH0ES (73.2 ± 1.3 km s⁻¹ Mpc⁻¹). Given that the tension between Planck and SH0ES data reaches approximately 4.17σ , our result significantly reduces the discrepancy by moving H_0 closer to the local value.

Each dataset exerts a distinct influence on the cosmological parameter constraints. The inclusion of CMB data (in D_1 and D_3) strongly affects the parameter uncertainties, particularly for Ω_{dm_0} , Ω_{r_0} , and $f\sigma_8$, due to their sensitivity to early-universe physics and background geometry. Conversely, the exclusion of CMB data in D_2 leads to broader parameter intervals and slight shifts in the matter and dark energy density parameters. Measurements of $f\sigma_8$ in D_1 and D_2 provide valuable information on the growth of cosmic structures and help constrain the parameters σ_8 and $f\sigma_8$. Comparisons involving dataset D_3 indicate that excluding $f\sigma_8$ data has a smaller impact than excluding CMB data. Finally, dataset D_4 , based on Planck and BAO data from reference [60], offers precise constraints on most parameters, especially σ_8 , and serves as an external benchmark to validate trends observed in D_1 through D_3 .

Comparison of dataset D_1 with D_2 and D_3

As seen in Table VII, a comparative analysis between the D_1 and D_2 datasets, within the flat Λ CDM framework, shows that while Ω_{Λ_0} differs by more than 2σ , the other primary parameters show deviations ranging from approximately 0.8σ to 1.7σ . Specifically, the deviations for Ω_{dm_0} , Ω_{b_0} , Ω_{Λ_0} , Ω_{r_0} , H_0 and σ_8 are approximately 1.67σ , 0.88σ , 3.37σ , 1.34σ , 1.12σ and 0.81σ , respectively. This emphasizes the crucial role of CMB data in accurately constraining not only the matter and dark energy densities but also the radiation component.

Next, we examine the influence of excluding $f\sigma_8$ data by comparing the D_1 and D_3 datasets, where D_3 corresponds to D_1 without $f\sigma_8$ data. The resulting shifts in parameter estimates are relatively small. The deviations for Ω_{dm_0} , Ω_{b_0} , Ω_{Λ_0} , Ω_{r_0} , and H_0 are approximately 0.50σ , less than 0.01σ , 0.48σ , 0.14σ , and 0.06σ , respectively (see Table VIII). These results indicate that, within the flat Λ CDM model, the cosmological parameters are primarily determined by CMB observations, while the contribution from σ_8 data remains relatively modest.

Comparison with D_4 dataset

In addition to our primary datasets (D_1 and D_3), we present the cosmological parameter constraints from the dataset D_4 , which is based on TT, TE, EE+lowE+lensing+ BAO data, as reported in Table 2 of [60]. Comparing our results with those from D_4 , we find that our estimates for key parameters such as Ω_{Λ_0} and H_0 are in broad agreement, with only minor deviations observed. The H_0 values from D_1 are consistent with those reported in D_4 within their respective uncertainties. On the other hand, the D_4 results yield a significantly higher value for σ_8 , which reflects differences in how large-scale structure data are incorporated into the analysis. These comparisons highlight the general consistency between our findings and those of D_4 , while also emphasizing the additional constraints provided by the combination of CMB and large-scale structure data.

After evaluating the differences between the datasets and analyzing the statistical models, we conclude that our approach shows good agreement with the results from D_4 in key parameters such as H_0 and Ω_{Λ_0} , while also offering new insights into the cosmological parameter space. The incorporation of additional observational data and refined fitting techniques contributes to improved precision in parameter estimation, making our framework a valuable tool for cosmological inference.

AIC and BIC analysis for flat Λ CDM model

To assess the statistical performance of the models under different dataset combinations, we evaluate the AIC and the BIC values reported in Table IV. Among the three primary datasets, D_3 yields the lowest AIC and BIC values (AIC = 1068.93, BIC = 1088.93), indicating the best trade-off between model fit and complexity. In contrast, D_2 (AIC

TABLE IV: The 68% confidence limits of flat Λ CDM model cosmological parameters (CPs) from D₁, D₂, D₃, and D₄ datasets. H_0 has units of $\text{km s}^{-1} \text{Mpc}^{-1}$. Here $\Omega_{m_0} = \Omega_{dm_0} + \Omega_{b_0}$.

CPs	D ₁	D ₂	D ₃	D ₄ [60]
Ω_{dm_0}	$0.2487^{+0.0050}_{-0.0063}$	0.228 ± 0.011	0.2521 ± 0.0037	—
Ω_{b_0}	0.0501 ± 0.0014	0.0461 ± 0.0043	$0.0501^{+0.0015}_{-0.0011}$	—
Ω_{m_0}	0.2988 ± 0.0071	0.2741 ± 0.0153	0.3022 ± 0.0050	0.3111 ± 0.0056
Ω_{Λ_0}	$0.7011^{+0.0066}_{-0.0053}$	0.726 ± 0.0043	0.6978 ± 0.0039	0.6889 ± 0.0056
Ω_{r_0}	$8.799^{+0.079}_{-0.012} \times 10^{-5}$	$10.061^{+0.55}_{-0.65} \times 10^{-5}$	$8.854^{+0.082}_{-0.11} \times 10^{-5}$	—
H_0	$67.27^{+0.86}_{-1.1}$	69.0 ± 1.2	$67.19^{+0.63}_{-0.99}$	67.66 ± 0.42
σ_8	$0.6423^{+0.0082}_{-0.0074}$	0.659 ± 0.019	—	0.8102 ± 0.0060
AIC	1086.75652	1081.18051	1068.92573	—
BIC	1111.75652	1106.18051	1088.92573	—

= 1081.18, BIC = 1106.18) and D₁ (AIC = 1086.76, BIC = 1111.76) exhibit higher values, suggesting that although D₁ includes the most comprehensive dataset, the penalty due to additional parameters leads to a comparatively less efficient fit. These comparisons highlight the statistical efficiency of models that balance data richness and model simplicity, and reinforce the importance of carefully selecting observational inputs.

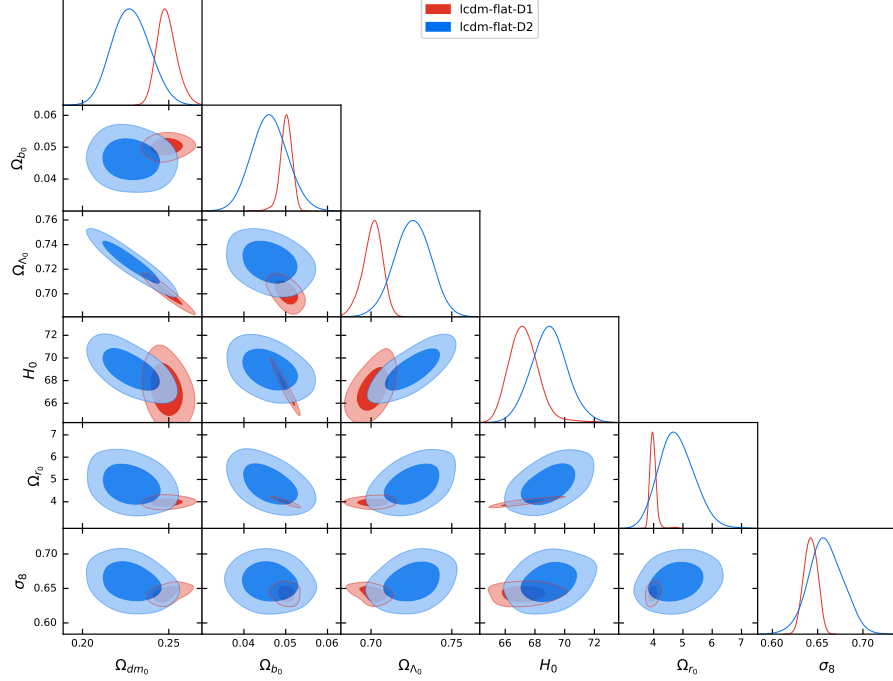


FIG. 1: One-dimensional likelihoods and 1σ and 2σ likelihood confidence contours of flat Λ CDM model parameters favored by D₁ and D₂ datasets.

2. Open Λ CDM model

The open Λ CDM model involves eight free parameters, constrained using different datasets. The corresponding results are presented in Tables V and VII, and illustrated in Figure 2.

The results indicate that the Hubble constant H_0 in the open Λ CDM model, for datasets D₁, D₂, and D₃, lies within the range of approximately 68.37 to $68.7 \text{ km s}^{-1} \text{Mpc}^{-1}$. These values show discrepancies of about 1.24σ , 1.08σ , and

0.92σ relative to the Planck 2018 estimate of $67.4 \pm 0.5 \text{ km s}^{-1} \text{ Mpc}^{-1}$, demonstrating close agreement with the Planck data. However, these values still significantly differ from the local SH0ES measurement, $73.2 \pm 1.3 \text{ km s}^{-1} \text{ Mpc}^{-1}$. The tension with dataset D_2 is approximately 2.64σ , and for D_1 and D_3 , it is around 3.17σ and 3.02σ , respectively. These findings suggest that introducing curvature in the open Λ CDM model partially alleviates the Hubble tension, even in datasets excluding CMB data (such as D_2), yet a significant discrepancy with local measurements remains.

The curvature parameter, Ω_{k_0} , is close to zero and slightly positive in D_1 and D_3 . In contrast, dataset D_2 exhibits larger uncertainty and a higher mean value of about 0.066, with substantial uncertainty, which increases the possibility of an open universe. The dark matter density, Ω_{dm_0} , and baryon density, Ω_{b_0} , remain relatively stable across datasets, around 0.23 and 0.048, respectively. The structure growth parameter, σ_8 is constrained using the D_1 and D_2 datasets and show significantly lower σ_8 values compared to other reported measurements. Statistical indicators, AIC and BIC, show that the open model with dataset D_3 attains the lowest values of these criteria and is thus statistically slightly favored over D_1 and D_2 .

Comparison of dataset D_1 with D_2 and D_3

We compare the D_1 and D_2 datasets within the open Λ CDM model to evaluate the impact of including CMB data. A comparative analysis reveals that all primary parameters differ by less than 2σ . Specifically, the deviations for Ω_{dm_0} , Ω_{b_0} , Ω_{k_0} , Ω_{Λ_0} , Ω_{r_0} , H_0 and σ_8 are approximately 1.33σ , 0.27σ , 1.3σ , 1.05σ , 1.85σ , 0.138σ and 1.15σ , respectively (see Table VII). This emphasizes the impact and importance of CMB data on constraining the matter, dark energy, and radiation densities.

To examine the effect of excluding $f\sigma_8$ data, we compare the D_1 and D_3 datasets. As shown in Tables VII and V, where D_3 corresponds to D_1 without $f\sigma_8$ data, the resulting shifts in parameter estimates are relatively small. The deviations for Ω_{dm_0} , Ω_{b_0} , Ω_{k_0} , Ω_{Λ_0} , Ω_{r_0} , and H_0 are approximately 0.026σ , 0.138σ , 0.093σ , 0.029σ , 0.08σ , and 0.129σ , respectively (see Table VII). These results suggest that, within the open Λ CDM model, the primary cosmological parameters are predominantly determined by the combination of CMB and other datasets, with relatively modest influence from $f\sigma_8$ data.

This suggests that the inclusion of $f\sigma_8$ data does not considerably improve the model statistical performance relative to the increase in parameter space complexity.

AIC and BIC analysis for open Λ CDM model

The AIC and BIC values for the open Λ CDM model are reported in Table V for the datasets D_1 , D_2 , and D_3 . These values give an indication of the relative model quality. For D_1 , the AIC is 1086.45 and the BIC is 1116.45. For D_2 , the AIC is 1083.23 and the BIC is 1113.23. Finally, for D_3 , the AIC is 1068.43 and the BIC is 1093.43. The lower AIC and BIC values for D_3 indicate a statistically more favorable fit for the open Λ CDM model when the $f\sigma_8$ data is omitted, implying that the inclusion of this dataset does not significantly enhance the model explanatory power relative to its complexity. The lower AIC and BIC values for D_3 indicate a statistically more favorable fit for the open Λ CDM model when the $f\sigma_8$ data are omitted, implying that the inclusion of this dataset does not significantly enhance the model explanatory power relative to its complexity.

3. Closed Λ CDM model

Cosmological parameter constraints for the seven parameter of closed Λ CDM model, derived from various datasets, are summarized in Tables VI and VII, and are shown in Figure 3. The Hubble parameter H_0 lies in the range of approximately 67 to $69.3 \text{ km s}^{-1} \text{ Mpc}^{-1}$. These values exhibit small deviations from the Planck 2018 result (67.4 ± 0.5), with discrepancies of 0.03σ , 1.7σ , and 0.52σ , respectively, indicating strong agreement with Planck data, particularly in the D_1 and D_3 datasets. However, these values show significant differences compared to the local SH0ES measurement (73.2 ± 1.3). The discrepancies are approximately 4.13σ and 4.38σ for D_1 and D_3 , respectively, indicating severe tension. In contrast, the D_2 dataset exhibits a smaller tension of about 2.37σ relative to SH0ES, although a statistically significant difference remains. While the tension between Planck and SH0ES is approximately 4.17σ .

The curvature parameter Ω_{k_0} is slightly negative and close to zero, indicating a mildly closed universe. The dark matter density parameter Ω_{dm_0} ranges roughly from 0.23 to 0.25, and the baryon density parameter Ω_{b_0} lies between approximately 0.045 and 0.05. The structure growth parameter, σ_8 is constrained using the D_1 and D_2 datasets and

TABLE V: The 68% confidence limits of open Λ CDM model cosmological parameters (CPs) from D_1 , D_2 , and D_3 datasets. H_0 has units of $\text{km s}^{-1} \text{Mpc}^{-1}$. Here $\Omega_{m_0} = \Omega_{dm_0} + \Omega_{b_0}$.

CPs	D_1	D_2	D_3
Ω_{dm_0}	$0.2318^{+0.0057}_{-0.0082}$	$0.206^{+0.021}_{-0.015}$	0.2315 ± 0.0087
Ω_{b_0}	$0.04817^{+0.00097}_{-0.0011}$	0.0469 ± 0.0046	0.0484 ± 0.0013
Ω_{k_0}	0.0051 ± 0.0020	$0.066^{+0.023}_{-0.060}$	0.0048 ± 0.0025
Ω_{Λ_0}	$0.7148^{+0.0074}_{-0.0053}$	$0.681^{+0.042}_{-0.021}$	0.7151 ± 0.0078
Ω_{r_0}	$8.204 \pm 0.087 \times 10^{-5}$	$10.66^{+0.57}_{-0.69} \times 10^{-5}$	$8.21 \pm 0.12 \times 10^{-5}$
H_0	$68.52^{+0.74}_{-0.64}$	68.7 ± 1.1	68.37 ± 0.93
σ_8	0.650 ± 0.013	$0.685^{+0.023}_{-0.032}$	—
AIC	1086.45093	1083.22539	1068.43036
BIC	1116.45093	1113.22539	1093.43036

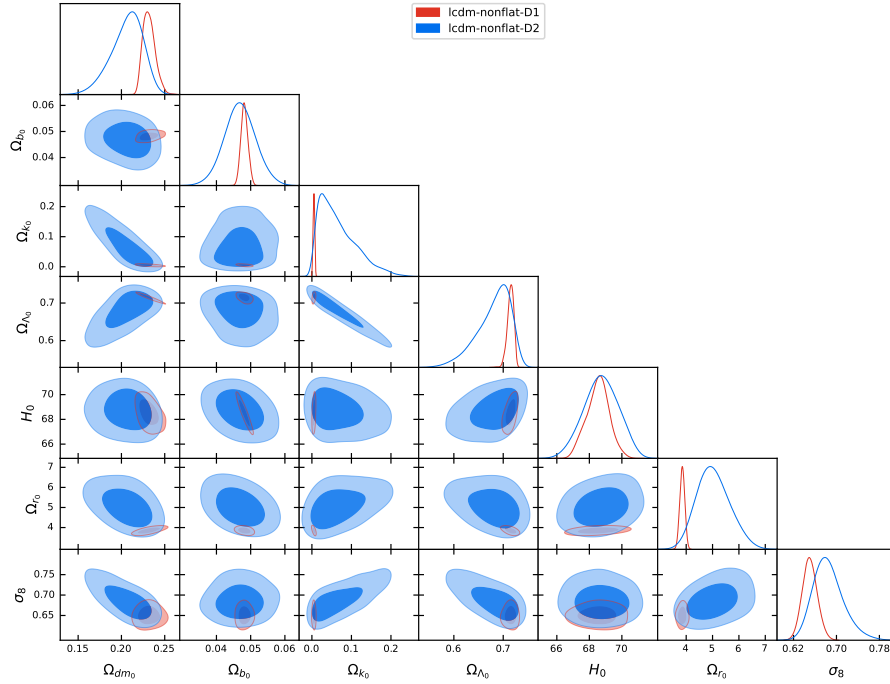


FIG. 2: One-dimensional likelihoods and 1σ and 2σ likelihood confidence contours of open Λ CDM ($\Omega_{k_0} > 0$) model parameters favored by D_1 and D_2 datasets.

show significantly lower σ_8 values compared to those obtained from the D_4 dataset and other reported measurements. Moreover, model selection criteria (AIC and BIC) indicate that the D_3 dataset provides the best fit.

Comparison of dataset D_1 with D_2 and D_3

We compare the results obtained from the D_1 and D_2 datasets within the closed Λ CDM model to investigate the impact of including CMB data. The comparison shows that the variations in most key parameters are less than 2σ , except for the parameter Ω_{Λ_0} , which exhibits a deviation of about 2.4σ . Specifically, the deviations for Ω_{dm_0} , Ω_{b_0} , Ω_{k_0} , Ω_{Λ_0} , Ω_{r_0} , H_0 and σ_8 are 1.01σ , 1.12σ , 1.36σ , 2.40σ , 1.47σ , 1.69σ and 0.03σ , respectively (see Table VII). This indicates that including CMB data in the closed Λ CDM model has a relatively modest effect on most parameters, but a significant impact on Ω_{Λ_0} .

TABLE VI: 68% confidence limits of closed Λ CDM model cosmological parameters (CPs) from D₁, D₂, and D₃ datasets. H_0 has units of $\text{km s}^{-1} \text{Mpc}^{-1}$. Here $\Omega_{m_0} = \Omega_{dm_0} + \Omega_{b_0}$.

CPs	D ₁	D ₂	D ₃
Ω_{dm_0}	$0.2485^{+0.0049}_{-0.0040}$	$0.236^{+0.010}_{-0.013}$	$0.2506^{+0.0054}_{-0.0062}$
Ω_{b_0}	0.05021 ± 0.00084	0.0454 ± 0.0042	$0.05065^{+0.00066}_{-0.00091}$
Ω_{k_0}	$-0.00187^{+0.0016}_{-0.00067}$	$-0.032^{+0.027}_{-0.017}$	$-0.00178^{+0.0016}_{-0.00063}$
Ω_{Λ_0}	0.7030 ± 0.0045	$0.750^{+0.017}_{-0.021}$	$0.7004^{+0.0064}_{-0.0056}$
Ω_{r_0}	$8.850^{+0.055}_{-0.029} \times 10^{-5}$	$9.97^{+0.41}_{-0.63} \times 10^{-5}$	$8.904 \pm 0.013 \times 10^{-5}$
H_0	67.38 ± 0.54	69.3 ± 1.0	$67.01^{+0.59}_{-0.51}$
σ_8	$0.650^{+0.016}_{-0.024}$	0.649 ± 0.020	—
AIC	1089.42136	1083.21688	1070.29891
BIC	1119.42136	1113.21688	1095.29891

To assess the influence of excluding σ_8 data, we compare the D₁ and D₃ datasets, where D₃ corresponds to D₁ without the $f\sigma_8$ data. This comparison reveals more significant shifts in certain cosmological parameters. Specifically, the variations in Ω_{dm_0} , Ω_{b_0} , Ω_{k_0} , Ω_{Λ_0} , Ω_{r_0} , and H_0 are 0.28σ , 0.38σ , 0.07σ , 0.34σ , 0.42σ , and 0.67σ , respectively (see Table VIII). These results suggest that excluding the σ_8 data significantly affects certain parameters, particularly Ω_{Λ_0} and H_0 .

AIC and BIC analysis for closed Λ CDM model

The AIC and BIC values for the closed Λ CDM model, summarized in Table VI for the D₁, D₂, and D₃ datasets, offer insight into the relative model quality. For D₁, the AIC is 1089.42, and the BIC is 1119.42. For D₂, the AIC is 1083.22, and the BIC is 1113.22. For D₃, the AIC is 1070.30, and the BIC is 1095.30. The lower AIC and BIC values for D₃ suggest that the closed Λ CDM model fits the data better when σ_8 data is excluded. This indicates that including σ_8 data does not substantially improve the model fitting to the datasets.

4. Assessment of geometrical models based on parameter consistency: The Λ CDM model

A comparative examination of the cosmological parameter differences between datasets D₁, D₂, and D₃ in Table VII allows us to evaluate the relative internal consistency of the flat, open, and closed Λ CDM scenarios. The differences are expressed in terms of the statistical deviation (σ) between dataset D₁ and the other combinations.

- Flat Λ CDM: Several parameters exhibit noticeable shifts between datasets, particularly in Ω_{Λ_0} and H_0 . The deviation of 3.37σ in Ω_{Λ_0} (D₁ compared to D₂) and 1.12σ in H_0 indicate a significant level of tension among the datasets when assuming a flat geometry.
- Open Λ CDM: The open model mostly shows moderate deviations. Except for Ω_{r_0} with a deviation of 1.85σ (D₁ compared to D₂), all other parameters remain within approximately 1.4σ . Notably, the parameters such as H_0 and Ω_{Λ_0} exhibit minimal shifts between D₁ and D₃. This suggests improved internal coherence across the observational datasets in this geometry. Moreover, consistency of the open model is further confirmed by the lower AIC and BIC values compared to the flat model, as shown in Table V.
- Closed Λ CDM: The closed case reveals intermediate parameter differences. In particular, Ω_{Λ_0} and H_0 deviate by 2.40σ and 1.69σ respectively (D₁ compared to D₂), exceeding the one sigma level. Although the closed model shows a better level of agreement than the flat model, it still falls short of the coherence seen in the open case. Incorporating curvature in this model helps us to reduce the discrepancies seen in the flat case but does not eliminate them entirely. The AIC and BIC values for the closed Λ CDM are slightly higher than those in the open model, further supporting the open geometry as the most consistent with the data.

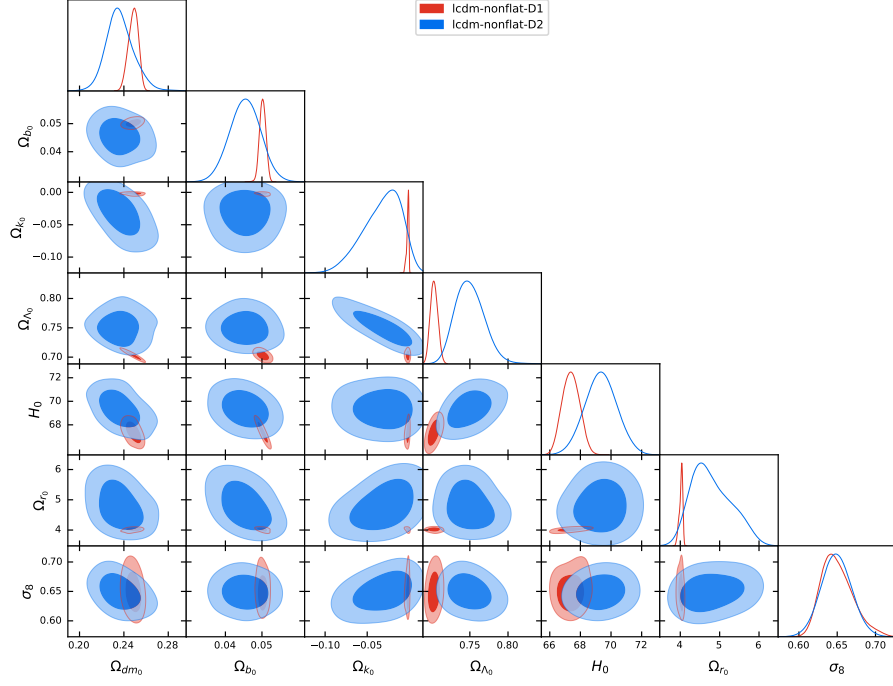


FIG. 3: One-dimensional likelihoods and 1σ and 2σ likelihood confidence contours of closed Λ CDM ($\Omega_{k0} < 0$) model parameters favored by D_1 and D_2 datasets.

TABLE VII: The cosmological parameter differences (CPD) for the Λ CDM model in flat and non-flat universe.

CPD	Λ CDM (Flat)		Λ CDM (Open)		Λ CDM (Closed)	
	$ D_1 - D_2 $	$ D_1 - D_3 $	$ D_1 - D_2 $	$ D_1 - D_3 $	$ D_1 - D_2 $	$ D_1 - D_3 $
Ω_{dm0}	1.67σ	0.50σ	1.33σ	0.026σ	1.01σ	0.28σ
Ω_{b0}	0.88σ	0.00σ	0.27σ	0.138σ	1.12σ	0.38σ
Ω_{k0}	—	—	1.30σ	0.093σ	1.36σ	0.07σ
$\Omega_{\Lambda0}$	3.37σ	0.48σ	1.05σ	0.029σ	2.40σ	0.34σ
Ω_{r0}	1.34σ	0.14σ	1.85σ	0.08σ	1.47σ	0.42σ
H_0	1.12σ	0.06σ	0.138σ	0.129σ	1.69σ	0.67σ
σ_8	0.81σ	—	1.15σ	—	0.03σ	—

These results highlight the sensitivity of cosmological parameter estimates to the assumed spatial curvature. Among the models considered, the open Λ CDM scenario appears to provide the most consistent constraints across independent dataset combinations, whereas the flat model shows the highest level of variation between the datasets. The inclusion of $f\sigma_8$ measurements, especially in the context of the open model, plays a crucial role in improving constraints on structure formation. Additionally, the statistical performance of the models, as indicated by AIC and BIC, confirms the superiority of open model in terms of data fit and simplicity.

B. Constraining the flat and non-flat models of R- Λ CDM

In this subsection, we investigate the R- Λ CDM model as a generalization of the standard cosmological scenario, considering spatially flat, open, and closed geometries. By employing various combinations of the previously introduced observational datasets, we constrain the cosmological parameters and assess the model's ability to account for the data. Our analysis explores the parameter space in light of current observations, with particular attention to possible deviations from the standard Λ CDM expectations. We further compare the resulting goodness-of-fit across different spatial curvatures and dataset combinations, and where applicable, quantify potential inconsistencies by employing the statistical tension estimator described in Appendix A. Finally, we summarize the inferred parameter constraints

and discuss the implications of spatial curvature in the context of this extended model.

1. *R- Λ CDM model in a flat universe*

In the flat R- Λ CDM framework, the deviation parameter ϵ , commonly referred to as the Rastall parameter, introduces a modification to the standard Λ CDM dynamics. This modification originates from the non-conservation of the matter energy-momentum tensor due to a non-minimal coupling between matter and geometry (for further details, see subsection II A). The results derived from this model, utilizing three distinct datasets D_1 , D_2 , and D_3 , are summarized in Table VIII and depicted in Figure 4.

The Hubble constant, H_0 , is consistently estimated to be approximately $69 \text{ km s}^{-1} \text{ Mpc}^{-1}$ across all datasets. The discrepancies between these estimates and those obtained from Planck and the local SH0ES measurements are summarized as follows: for dataset D_1 , approximately 1.69σ and 2.61σ , respectively; for D_2 , about 1.38σ and 2.26σ ; and for D_3 , around 1.37σ and 2.52σ . These results indicate that the R- Λ CDM model significantly alleviates the existing Hubble tension, reducing the deviations to below the 3σ threshold relative to both reference datasets. This outcome suggests a comparatively improved consistency in estimating the cosmic expansion rate compared to the canonical Λ CDM model.

The dark matter density parameter, Ω_{dm_0} , is found to be nearly identical, approximately 0.235, in datasets D_1 and D_3 . In contrast, in dataset D_2 , from which CMB data have been excluded, the mean value rises to roughly 0.323 accompanied by an increased uncertainty. This observation emphasizes the pivotal role of CMB measurements in tightly constraining the dark matter density.

Similarly, the baryonic matter density parameter, Ω_{b_0} , remains approximately constant at about 0.047 across all datasets, albeit with a slightly elevated uncertainty in D_2 . The dark energy density parameter, Ω_{Λ_0} , is estimated at approximately 0.728 in D_1 and D_3 , while it reaches around 0.878 in D_2 . The radiation density parameter, Ω_{r_0} , is negligible in all datasets, on the order of $4 \times 10^{-5} h^{-2}$, but exhibits greater uncertainty in D_2 .

The Rastall deviation parameter, ϵ , assumes small negative values close to zero (approximately -0.002) in datasets D_1 and D_3 . Conversely, in D_2 , it attains a more significant negative value with larger uncertainty (approximately -0.115), indicating the significant impact of excluding CMB data on its estimation.

The parameter σ_8 , which characterizes the amplitude of matter fluctuations, is reported only for datasets D_1 and D_2 . Its estimated value is around 0.67, which is lower than the corresponding value reported by Planck.

Finally, information criteria, namely AIC and BIC, suggest that the model calibrated with dataset D_3 attains lower values of these criteria, thereby indicating a potentially superior fit to the corresponding observational data.

Comparison of dataset D_1 with D_2 and D_3

The comparison of constrained parameters derived from the D_1 and D_2 datasets in the flat R- Λ CDM model reveals notable differences across several parameters. For example, the dark matter density parameter, Ω_{dm_0} , shows a substantial shift of 3.35σ , indicating a higher value in D_2 . Similarly, the radiation density Ω_{r_0} and the cosmological constant Ω_{Λ_0} exhibit deviations of 2.20σ and 1.87σ , respectively, favoring a higher energy density in D_2 . The parameter ϵ also shows a marked deviation of 2.09σ , indicating a larger deviation from the standard Λ CDM dynamics. The Hubble constant H_0 remains nearly consistent across both datasets. These discrepancies, illustrated in Table XIV, may reflect the impact of differing data combinations, particularly the absence of CMB in D_2 , on the sensitivity of cosmological parameter estimates.

The cosmological parameters derived from the D_1 and D_3 datasets, which both include BBN, H, BAO, SN, and CMB, show a high degree of internal consistency in the flat R- Λ CDM model. No significant deviations are observed across the primary parameters, such as Ω_{dm_0} , Ω_{b_0} , Ω_{Λ_0} , and H_0 , with differences less than 0.16σ . The parameter ϵ and radiation density Ω_{r_0} also show minimal changes, falling within the statistical uncertainties. The value of σ_8 is not available in D_3 , but the overall parameter space indicates strong consistency. As indicated in Table XIV, this consistency highlights the stability of the combined observational constraints from D_1 and D_3 , and indicates statistical agreement within 0.16σ , reflecting strong consistency in parameter estimates.

AIC and BIC analysis

To evaluate the relative performance of the flat R- Λ CDM model, the AIC and BIC values were calculated for the dataset combinations D_1 , D_2 , and D_3 (Table IX). Among these, the D_3 dataset provides the lowest AIC and BIC

TABLE VIII: The 68% confidence limits of flat R- Λ CDM model cosmological parameters (CPs) from D₁, D₂, and D₃ datasets. H_0 has units of $\text{km s}^{-1} \text{Mpc}^{-1}$. Here $\Omega_{m_0} = \Omega_{dm_0} + \Omega_{b_0}$.

CPs	D ₁	D ₂	D ₃
Ω_{dm_0}	$0.2352^{+0.0084}_{-0.0069}$	$0.323^{+0.035}_{-0.015}$	0.2349 ± 0.0083
Ω_{b_0}	$0.04725^{+0.00092}_{-0.0016}$	0.0460 ± 0.0045	$0.0475^{+0.0016}_{-0.0012}$
Ω_{Λ_0}	$0.728^{+0.011}_{-0.015}$	$0.878^{+0.10}_{-0.058}$	$0.728^{+0.013}_{-0.015}$
Ω_{r_0}	$8.7^{+0.095}_{-0.11} \times 10^{-5}$	$16.3^{+2.3}_{-1.0} \times 10^{-5}$	$8.69^{+0.075}_{-0.11} \times 10^{-5}$
ϵ	$-0.00202^{+0.0011}_{-0.00094}$	$-0.115^{+0.044}_{-0.064}$	$-0.00195^{+0.0011}_{-0.00087}$
H_0	$69.1^{+1.1}_{-0.65}$	69.2 ± 1.2	$68.99^{+0.89}_{-1.2}$
σ_8	0.6692 ± 0.0091	0.658 ± 0.019	—
AIC	1085.87680	1083.19308	1067.84826
BIC	1115.87680	1113.19308	1092.84826

TABLE IX: Comparison of AIC and BIC values between flat-universe R- Λ CDM and Λ CDM models for datasets D₁, D₂, and D₃. The differences ΔAIC and ΔBIC are calculated as R- Λ CDM minus Λ CDM.

Dataset	AIC			BIC		
	Λ CDM	R- Λ CDM	ΔAIC	Λ CDM	R- Λ CDM	ΔBIC
D ₁	1086.76	1085.88	0.88	1111.76	1115.88	4.12
D ₂	1081.18	1083.19	2.01	1106.18	1113.19	7.01
D ₃	1068.93	1067.85	1.08	1088.93	1092.85	3.92

values, indicating the best balance between model fit and complexity. This improvement may be partially due to the exclusion of $f\sigma_8$ data, which can reduce tensions related to structure growth.

The ΔAIC values suggest a marginal preference (with $|\Delta\text{AIC}| < 2$) for the R- Λ CDM model in datasets D₁ and D₃, where negative differences ($\Delta\text{AIC} = -0.88$ and -1.08 , respectively) indicate a slightly better fit compared to the standard Λ CDM model. In contrast, dataset D₂ yields a positive ΔAIC of $+2.01$, suggesting a marginally better performance for the Λ CDM model in the absence of CMB data.

Regarding BIC, which imposes a stronger penalty on model complexity, all datasets show higher values for the R- Λ CDM model, with ΔBIC ranging from $+3.92$ to $+7.01$. These consistent increases indicate that the standard Λ CDM model is generally preferred from the viewpoint of simplicity. According to standard model selection criteria, a ΔBIC greater than 6 is generally interpreted as strong evidence against the more complex model.

In summary, while the AIC provides limited support for the R- Λ CDM model in two of the three dataset combinations, the BIC generally favors the standard Λ CDM model due to its simpler structure. These results emphasize the significant impact of dataset composition, particularly the inclusion or exclusion of CMB and $f\sigma_8$ data, on the statistical evaluation of cosmological models. Overall, despite the presence of an additional parameter, the R- Λ CDM model achieves marginal improvements in fit for certain dataset combinations, suggesting its potential to better capture some cosmological features.

2. R- Λ CDM model in an open universe

The cosmological parameter estimates for the eight-parameter open R- Λ CDM model, obtained using datasets D₁, D₂, and D₃, are summarized in Table X and illustrated in Figure 5.

The Hubble constant H_0 is estimated to be 68.92 ± 0.38 , $68.8^{+1.2}_{-0.86}$, and $68.3 \pm 1.2 \text{ km s}^{-1} \text{Mpc}^{-1}$ for datasets D₁, D₂, and D₃, respectively. These values are above the Planck 2018 reference ($67.4 \pm 0.5 \text{ km s}^{-1} \text{Mpc}^{-1}$) but below the local SH0ES measurement ($73.2 \pm 1.3 \text{ km s}^{-1} \text{Mpc}^{-1}$).

In the standard flat Λ CDM model, the tension between the Hubble constant inferred from Planck data and the local SH0ES measurement is approximately 4.17σ . In the open universe R- Λ CDM model, the tension between the inferred values of H_0 from this model and the Planck data is significantly reduced to about 2.42σ , 1.22σ , and 0.69σ for datasets D₁, D₂, and D₃, respectively. Similarly, the tension with the local SH0ES measurement decreases to approximately

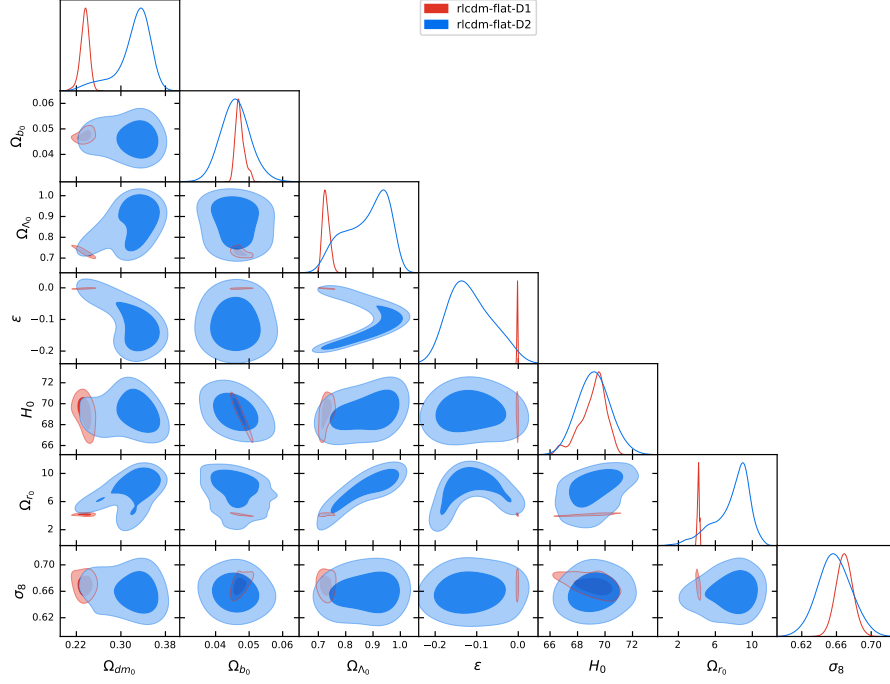


FIG. 4: One-dimensional likelihoods and 1σ and 2σ likelihood confidence contours of flat R- Λ CDM model parameters favored by D_1 and D_2 datasets.

3.16σ , 2.65σ , and 2.77σ for the same datasets.

Regarding other parameters, the dark matter density Ω_{dm0} is nearly identical for D_1 and D_3 at around 0.23, but increases to about 0.297 in D_2 , likely reflecting the absence of CMB data in this dataset. The baryonic matter density Ω_{b0} remains stable around 0.047 across all datasets.

The spatial curvature parameter Ω_{k0} is positive but small, with the largest value and uncertainty found in D_2 (approximately 0.064). The dark energy density $\Omega_{\Lambda0}$ is about 0.70 in D_1 and D_3 , rising to nearly 0.81 in D_2 . Radiation density Ω_{r0} is very low ($\sim 10^{-5}h^{-2}$) for all datasets, with a higher value and uncertainty in D_2 .

The Rastall deviation parameter ϵ is positive and near zero in D_1 and D_3 , but negative and more uncertain (around -0.125) in D_2 . The cosmic structure growth parameter σ_8 is reported only for D_1 and D_2 , with values near 0.67. Finally, AIC and BIC analyses indicate the best model fit with dataset D_3 , as these criteria attain their lowest values there.

Comparison of dataset D_1 with D_2 and D_3

Comparing parameters from D_1 and D_2 reveals notable deviations in Ω_{dm0} and Ω_{r0} exceeding 2σ (approximately 2.37σ and 2.11σ respectively), suggesting tension likely due to the exclusion of CMB data in D_2 . Differences in Ω_{b0} and $\Omega_{\Lambda0}$ are smaller, under 1.5σ . The curvature parameter Ω_{k0} differs by about 1.41σ , and the ϵ parameter shows a significant deviation of 2.95σ . Most other parameters are consistent within uncertainties. Detailed values are provided in Table XIV.

Parameters derived from D_1 and D_3 datasets show strong agreement, with all differences below 0.5σ . The largest offsets are found in H_0 (0.49σ) and ϵ (0.27σ), while others such as Ω_{dm0} , Ω_{b0} , $\Omega_{\Lambda0}$, and Ω_{k0} exhibit minimal, statistically insignificant variations. It is likely due to the presence of CMB data in datasets D_1 and D_3 , and its absence in D_2 . Overall, parameter estimates from both datasets are consistent within the open universe R- Λ CDM framework. Further details can be found in Table XIV.

TABLE X: The 68% confidence limits of open R- Λ CDM model cosmological parameters (CPs) from D₁, D₂, and D₃ datasets. H_0 has units of $\text{km s}^{-1} \text{Mpc}^{-1}$. Here $\Omega_{m_0} = \Omega_{dm_0} + \Omega_{b_0}$.

CPs	D ₁	D ₂	D ₃
Ω_{dm_0}	$0.2241^{+0.0022}_{-0.0069}$	$0.297^{+0.037}_{-0.024}$	$0.229^{+0.013}_{-0.011}$
Ω_{b_0}	$0.04768^{+0.00070}_{-0.00085}$	0.0468 ± 0.0049	0.0486 ± 0.0018
Ω_{k_0}	$0.0086^{+0.0046}_{-0.0070}$	$0.064^{+0.024}_{-0.054}$	$0.0095^{+0.0041}_{-0.0088}$
Ω_{Λ_0}	$0.700^{+0.012}_{-0.018}$	0.813 ± 0.081	$0.702^{+0.020}_{-0.025}$
Ω_{r_0}	$7.45^{+0.14}_{-0.28} \times 10^{-5}$	$16.9^{+2.4}_{-1.8} \times 10^{-5}$	$7.69 \pm 0.31 \times 10^{-5}$
ϵ	$0.0038^{+0.0046}_{-0.0031}$	$-0.125^{+0.026}_{-0.061}$	$0.0021^{+0.0053}_{-0.0045}$
H_0	68.92 ± 0.38	$68.8^{+1.2}_{-0.86}$	68.3 ± 1.2
σ_8	0.6678 ± 0.0031	$0.688^{+0.019}_{-0.025}$	—
AIC	1087.74371	1085.35573	1069.36801
BIC	1122.74371	1120.35573	1099.36801

TABLE XI: Comparison of AIC and BIC values between open-universe R- Λ CDM and Λ CDM models for datasets D₁, D₂, and D₃. The differences ΔAIC and ΔBIC are calculated as R- Λ CDM minus Λ CDM.

Dataset	AIC			BIC		
	Λ CDM	R- Λ CDM	ΔAIC	Λ CDM	R- Λ CDM	ΔBIC
D ₁	1086.45	1087.74	1.29	1116.45	1122.74	6.29
D ₂	1083.23	1085.36	2.13	1113.23	1120.36	7.13
D ₃	1068.43	1069.37	0.94	1093.43	1099.37	5.94

AIC and BIC analysis

The relative performance of the open R- Λ CDM model was evaluated using AIC and BIC for datasets D₁, D₂, and D₃. Both criteria favor D₃ for the best balance between fit and complexity, yielding the lowest values. Dataset D₂, lacking CMB data, performs worst, highlighting the importance of CMB constraints for parameter estimation and model selection.

Table X compares AIC and BIC between the open R- Λ CDM and standard Λ CDM models. Positive differences (ΔAIC and ΔBIC , computed as R- Λ CDM minus Λ CDM) across datasets reflect the penalty for increased model complexity. ΔAIC ranges from about +0.94 (D₃) to +2.13 (D₂), while ΔBIC spans 5.94 to 7.13, indicating stronger penalization by BIC.

Although the simpler Λ CDM model is statistically favored by current data, the open R- Λ CDM model remains a viable alternative, with ΔAIC values below 2 commonly interpreted as statistically indistinguishable. This analysis emphasizes the trade-off between goodness of fit and model complexity in cosmology.

3. R- Λ CDM model in a closed universe

Table XII summarizes the cosmological parameter estimates of the eight parameter R- Λ CDM model assuming a closed universe geometry (negative curvature). These results are derived from three independent observational datasets (D₁, D₂, and D₃) and are also illustrated in Figure 6.

The estimated values of the Hubble constant H_0 in the closed R- Λ CDM model are 69.3 ± 1.1 , $69.7^{+1.1}_{-1.3}$, and $68.7^{+1.8}_{-1.3}$ km/s/Mpc for datasets D₁, D₂, and D₃, respectively. These values are higher than the Planck 2018 measurement and lower than the local SH0ES measurement. Furthermore, they are in good agreement with the Atacama Cosmology Telescope (ACT) results, which reported $68.22 \pm 0.36 \text{ km s}^{-1} \text{Mpc}^{-1}$, with discrepancies less than 1σ [124–126].

The tension between the H_0 values inferred from the model and Planck data which was approximately 4.17σ in the standard flat Λ CDM model when compared to local SH0ES measurements [127] is significantly reduced to about 1.58σ , 1.77σ , and 0.80σ for datasets D₁, D₂, and D₃, respectively. Similarly, the tension with the local SH0ES measurements decreases but remains significant, at approximately 2.29σ , 1.97σ , and 2.18σ for the same datasets.

The dark matter density parameter Ω_{dm_0} ranges approximately from 0.24 to 0.365, with the highest value observed

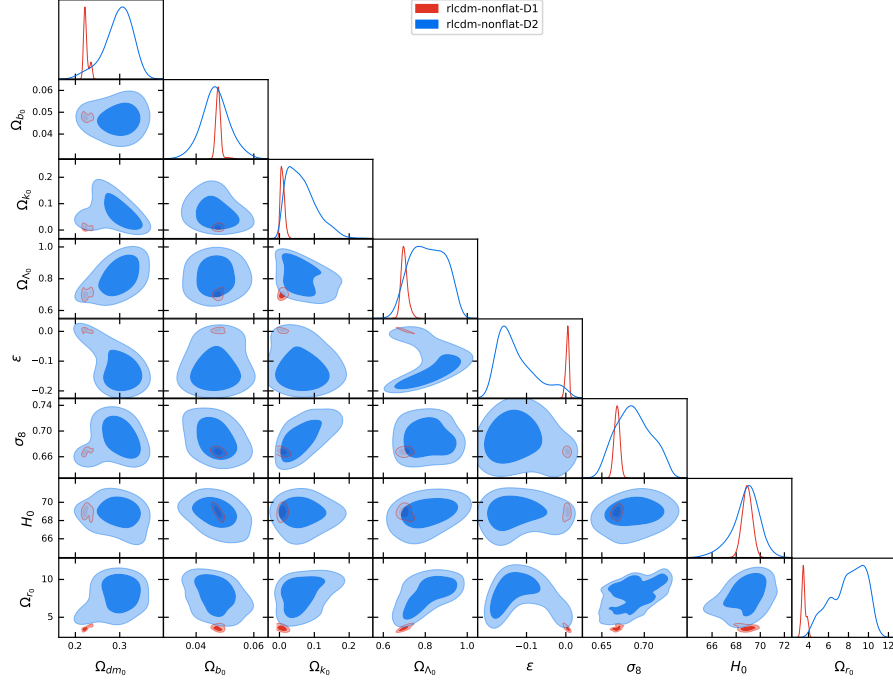


FIG. 5: One-dimensional likelihoods and 1σ and 2σ likelihood confidence contours of open R- Λ CDM ($\Omega_{k_0} > 0$) model parameters favored by D₁ and D₂ datasets.

in D₂ and similar values in D₁ and D₃. The baryon density Ω_{b_0} remains nearly constant, between 0.045 and 0.048. The spatial curvature parameter Ω_{k_0} is negative, indicating a closed spatial geometry; the most significant negative value is observed in D₂ (around -0.083), with a larger uncertainty. The dark energy density Ω_{Λ_0} varies between 0.72 and 0.77, with a slightly higher estimate in D₂. The radiation density Ω_{r_0} is very small, but it shows a larger value and greater uncertainty.

The Rastall parameter ϵ is close to zero and negative in D₁ and D₃, but more negative and less constrained in D₂. The structure growth parameter σ_8 is reported only for D₁ and D₂, with slightly higher values in D₁. The information criteria AIC and BIC indicate that the best fit corresponds to dataset D₃, as these criteria attain their lowest values in this dataset.

Overall, assuming a closed geometry, the cosmological parameters are estimated within reasonable ranges and show fluctuations consistent with the types of datasets used. Most differences in parameters between datasets are within 2σ , indicating general agreement. However, some parameters, such as Ω_{dm_0} and ϵ , show differences slightly exceeding 2σ , mainly between datasets D₁ and D₂, whereas the differences between D₁ and D₃ remain minimal (e.g., the difference in Ω_{dm_0} is about 0.34σ), reflecting closer agreement between these two datasets (see Table XIV).

Comparison of dataset D₁ with D₂ and D₃

The differences in cosmological parameters derived from the D₁ and D₂ datasets for the closed R- Λ CDM model are summarized in Table XIV. The most prominent deviation is observed in the dark matter density parameter Ω_{dm_0} , which exhibits a significant difference of 2.92σ , indicating a notable discrepancy between these datasets. Small differences are seen in the Hubble constant H_0 (ΔH_0 : 0.24σ) and the baryon density ($\Delta\Omega_{b_0}$: 0.40σ) parameters. These differences suggest a more significant closed spatial curvature inferred from D₂, potentially due to differences in the observational probes employed. The cosmological constant Ω_{Λ_0} differs by 0.49σ , whereas the parameter ϵ shows a substantial deviation of 2.30σ , indicating significant variation in cosmic evolution between the datasets. Additionally, the clustering amplitude σ_8 shifts by 1.52σ . These results underscore the impact of dataset composition on parameter estimation, especially in the comparison of D₁ and D₂. The radiation density parameter Ω_{r_0} shows a significant deviation of approximately 2.84σ between D₁ and D₂. This reflects a meaningful difference in the estimated radiation content across these datasets.

A similar comparison between D₁ and D₃ is presented in Table XIV, revealing more subtle differences. The dark

TABLE XII: The 68% confidence limits of closed R- Λ CDM model cosmological parameters (CPs) from D₁, D₂, and D₃ datasets. H_0 has units of $\text{km s}^{-1} \text{Mpc}^{-1}$. Here $\Omega_{m_0} = \Omega_{dm_0} + \Omega_{b_0}$.

CPs	D ₁	D ₂	D ₃
Ω_{dm_0}	0.244 ± 0.014	0.365 ± 0.039	$0.251^{+0.013}_{-0.017}$
Ω_{b_0}	0.0471 ± 0.0015	0.0452 ± 0.0045	$0.0480^{+0.0017}_{-0.0026}$
Ω_{k_0}	$-0.0241^{+0.011}_{-0.0081}$	$-0.083^{+0.068}_{-0.036}$	-0.0232 ± 0.0057
Ω_{Λ_0}	0.723 ± 0.031	$0.773^{+0.11}_{-0.083}$	0.722 ± 0.021
Ω_{r_0}	$10.64^{+0.27}_{-0.19} \times 10^{-5}$	$17.1 \pm 1.1 \times 10^{-5}$	$10.884 \pm 0.060 \times 10^{-5}$
ϵ	-0.0076 ± 0.0067	$-0.102^{+0.036}_{-0.045}$	-0.0089 ± 0.0042
H_0	69.3 ± 1.1	$69.7^{+1.1}_{-1.3}$	$68.7^{+1.8}_{-1.3}$
σ_8	$0.6682^{+0.0064}_{-0.0053}$	$0.630^{+0.026}_{-0.023}$	—
AIC	1086.12777	1085.15656	1067.23879
BIC	1121.12777	1120.15656	1097.23879

TABLE XIII: Comparison of AIC and BIC values between closed-universe R- Λ CDM and Λ CDM models for datasets D₁, D₂, and D₃. The differences ΔAIC and ΔBIC are calculated as R- Λ CDM minus Λ CDM.

Dataset	AIC			BIC		
	Λ CDM	R- Λ CDM	ΔAIC	Λ CDM	R- Λ CDM	ΔBIC
D ₁	1089.42	1086.13	3.29	1119.42	1121.13	1.71
D ₂	1083.22	1085.16	1.94	1113.22	1120.16	6.94
D ₃	1070.30	1067.24	3.06	1095.30	1097.24	1.94

matter density parameter Ω_{dm_0} differs by only 0.34σ , indicating closer agreement relative to D₁ and D₂. The baryon density parameter Ω_{b_0} also remains consistent, with a difference of 0.34σ . The spatial curvature parameter Ω_{k_0} shows a negligible shift of 0.08σ , consistent with the fact that both datasets include CMB data. Similarly, the cosmological constant Ω_{Λ_0} and the parameter ϵ differ by 0.03σ and 0.16σ , respectively. The Hubble constant H_0 varies slightly by 0.32σ . The radiation density parameter Ω_{r_0} differs by approximately 0.01σ , showing a negligible difference between D₁ and D₃. These results confirm a high level of consistency between D₁ and D₃ within the closed universe model.

AIC and BIC analysis

Table XIII presents a comparative assessment of model selection criteria, including the AIC and BIC, for the closed R- Λ CDM model. These criteria quantify the balance between model accuracy and complexity.

Among the three dataset combinations, D₃ yields the lowest AIC and BIC values, indicating the most favorable trade-off between goodness of fit and model simplicity. This advantage primarily arises from excluding the $f\sigma_8$ data in D₃, which mitigates tensions between structure growth and background evolution constraints.

The differences between D₁ and D₃ are moderate ($\Delta\text{AIC} \approx 3.06$, $\Delta\text{BIC} \approx 1.94$), slightly favoring D₃. Dataset D₂, which lacks CMB data, performs less favorably in both criteria, emphasizing the essential role of CMB observations in constraining cosmological parameters.

Table VI compares the closed R- Λ CDM model with the standard closed Λ CDM model. For D₁ and D₃, the R- Λ CDM model achieves slightly lower AIC values compared to the standard Λ CDM, indicating a marginally better fit. However, the BIC values remain consistently higher due to the additional Rastall parameter, thus favoring the simpler model.

In summary, D₃ yields the best overall performance within the closed R- Λ CDM framework, benefiting from reduced tension due to the exclusion of $f\sigma_8$ data. While the AIC favors the Rastall extension for its better fit, the BIC remains conservative, consistently preferring the simpler Λ CDM model. These results highlight the value of combining diverse observational datasets and employing rigorous model selection criteria to improve the robustness and precision of cosmological inferences.

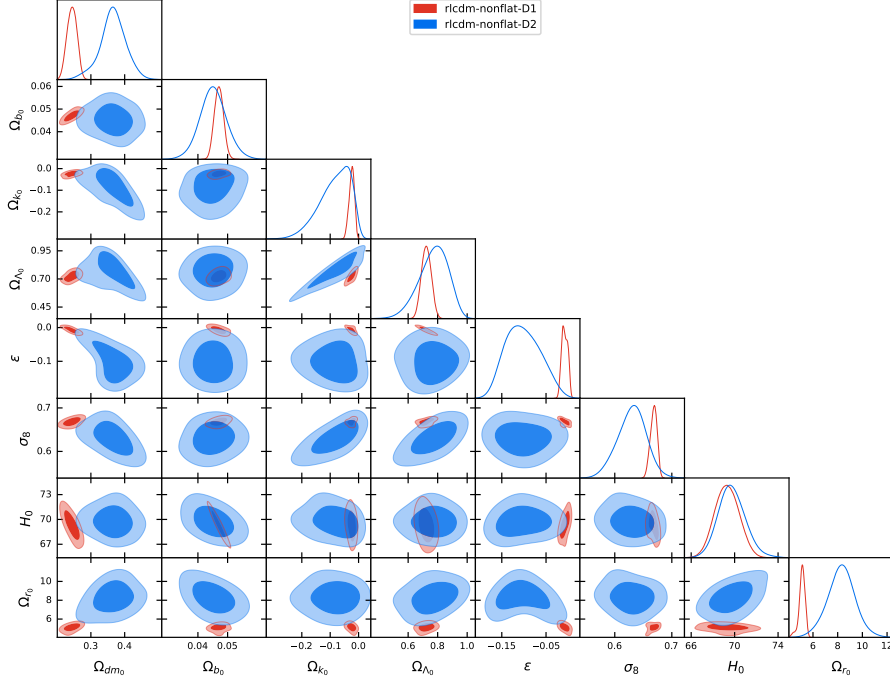


FIG. 6: One-dimensional likelihoods and 1σ and 2σ likelihood confidence contours of closed R- Λ CDM ($\Omega_{k_0} < 0$) model parameters favored by D₁ and D₂ datasets.

4. Assessment of geometrical models based on parameter consistency: The R- Λ CDM case

A comparative assessment of the differences in cosmological parameters among the data sets D₁, D₂, and D₃ in Table XIV allows us to evaluate the relative consistency of different geometric scenarios within the R- Λ CDM model. The differences are expressed in terms of statistical deviations (σ) between data set D₁ and other combinations.

- **Flat R- Λ CDM Model:** In this scenario, the parameter Ω_{dm_0} shows the largest inconsistency with a deviation of 3.35σ (between D₁ and D₂), indicating a significant discrepancy in the dark matter density between the two data sets. Additionally, the parameter Ω_{r_0} with 2.20σ and ϵ with 2.09σ also exhibit notable deviations. In contrast, the parameters such as H_0 with only -0.067σ and Ω_{Λ_0} with 1.87σ show lower levels of inconsistency. Overall, this model demonstrates lower compatibility among the data, especially regarding matter and radiation density parameters.
- **Open R- Λ CDM Model:** In the open model, deviations in most parameters are reduced, indicating better internal consistency among the data sets. The most significant deviation appears in ϵ with 2.95σ , which may signal a sensitive dependence of this parameter on the spatial geometry. Other parameters, such as H_0 (0.11σ), Ω_{Λ_0} (1.37σ), and $f\sigma_8$ (0.373σ), show only minor differences between D₁ and D₂. This suggests that the open R- Λ CDM model provides acceptable coherence among the data.
- **Closed R- Λ CDM Model:** Similarly to the open model, inconsistencies are generally reduced in this model, although some parameters still show deviations. Specifically, Ω_{dm_0} with 2.92σ and ϵ with 2.30σ exhibit the largest differences between D₁ and D₂. On the other hand, parameters such as H_0 with only 0.24σ and Ω_{Λ_0} with 0.49σ show good agreement. The value of H_0 in this model is found to be approximately $69.7^{+1.1}_{-1.3}$, which is higher than the corresponding value from Planck data and closer to local measurements (e.g., SH0ES) (see Table XII). This feature indicates that the closed model has been able to alleviate part of the Hubble tension.

VI. CONCLUSIONS

In this study, we investigated the performance of the standard cosmological model, Λ CDM, and its extended version, R- Λ CDM, under different spatial geometries (flat, open, and closed), using a comprehensive set of observational data.

TABLE XIV: The cosmological parameter differences (CPD) for the R- Λ CDM model in flat and non-flat universe.

CPD	R- Λ CDM (Flat)		R- Λ CDM (Open)		R- Λ CDM (Closed)	
	$ \mathbf{D}_1 - \mathbf{D}_2 $	$ \mathbf{D}_1 - \mathbf{D}_3 $	$ \mathbf{D}_1 - \mathbf{D}_2 $	$ \mathbf{D}_1 - \mathbf{D}_3 $	$ \mathbf{D}_1 - \mathbf{D}_2 $	$ \mathbf{D}_1 - \mathbf{D}_3 $
Ω_{dm_0}	3.35σ	0.026σ	2.37σ	0.38σ	2.92σ	0.34σ
Ω_{b_0}	0.267σ	0.132σ	0.18σ	0.47σ	0.40σ	0.34σ
Ω_{k_0}	—	—	1.41σ	0.10σ	1.11σ	0.08σ
Ω_{Λ_0}	1.87σ	0.00σ	1.37σ	0.07σ	0.49σ	0.03σ
Ω_{r_0}	2.20σ	0.159σ	2.11σ	0.13σ	2.84σ	0.01σ
ϵ	2.09σ	0.049σ	2.95σ	0.27σ	2.30σ	0.16σ
H_0	0.067σ	0.080σ	0.11σ	0.49σ	0.24σ	0.32σ
σ_8	0.531σ	—	0.91σ	—	1.52σ	—

The main objective was to evaluate the ability of these models to alleviate the well-known Hubble tension (H_0). Our analysis utilized a wide range of data, including BBN, measurements of the Hubble parameter $H(z)$ over the redshift range $0.07 \leq z \leq 2.36$, BAO, Type Ia Supernovae, CMB data from Planck 2018 and ACT 2025, as well as galaxy clustering data via the $f\sigma_8$ parameter. Statistical inference was performed using the MCMC method, and model selection was carried out via the AIC and BIC.

In the flat Λ CDM model, the inferred H_0 values ranged from 67.2 to $69.0 \text{ km s}^{-1} \text{ Mpc}^{-1}$, consistent with the Planck estimation ($67.4 \pm 0.5 \text{ km s}^{-1} \text{ Mpc}^{-1}$), but remaining significantly in tension with the SH0ES local measurement ($73.2 \pm 1.3 \text{ km s}^{-1} \text{ Mpc}^{-1}$), leading to a discrepancy at the level of about 2.37σ to 3.9σ . Hence, the H_0 tension remains unresolved in this framework.

Examining the open and closed geometries within the Λ CDM framework revealed that the open model improves data consistency and is statistically favored by both AIC and BIC analysis. In this model, the tension with SH0ES is reduced to approximately 3.17σ , 2.64σ , and 3.02σ for \mathbf{D}_1 , \mathbf{D}_2 , and \mathbf{D}_3 , respectively. In the closed model, while the tension remains high for \mathbf{D}_1 and \mathbf{D}_2 (4.13σ and 4.38σ), it significantly decreases to about 2.37σ for \mathbf{D}_3 . Nevertheless, this reduction is still insufficient to fully resolve the Hubble tension in most cases.

Next, we analyzed the R- Λ CDM model, in which a new parameter ϵ accounts for a non-minimal coupling between matter and geometry. This model exhibited better performance in reducing the tensions, particularly in non-flat geometries. In the flat R- Λ CDM model, the Hubble constant H_0 is consistently estimated to be approximately $69 \text{ km s}^{-1} \text{ Mpc}^{-1}$ across all datasets. The tension with the Planck and SH0ES measurements is significantly reduced to the range of 1.37σ – 1.69σ and 2.26σ – 2.61σ , respectively.

Further improvements are observed in the closed R- Λ CDM model. Across the three datasets, the tension between the H_0 values and Planck data lies in the range 0.80σ – 1.77σ , while the discrepancy with the local SH0ES measurement is reduced to 1.97σ – 2.18σ . Compared to the standard flat Λ CDM model, where the Planck–SH0ES discrepancy is around 4.17σ [127], these results represent a substantial and consistent reduction in the Hubble tension. Although the open R- Λ CDM model achieves even smaller discrepancies with Planck (down to 0.69σ), it shows larger deviations with SH0ES (up to 3.17σ). Therefore, the closed geometry offers the most balanced resolution of the H_0 tension when considering both datasets simultaneously.

These results indicate that the extended R- Λ CDM model, particularly in non-flat geometries, has made substantial progress in bridging the historical gap between cosmological (Planck and ACT) and local (SH0ES) data. Notably, the Planck–SH0ES discrepancy stands at about 4.17σ .

The R- Λ CDM model in the closed geometry shows a significant improvement in the statistical criteria AIC and BIC compared to the standard Λ CDM model for datasets \mathbf{D}_1 and \mathbf{D}_3 (with ΔAIC greater than 3), while the complexity penalty of BIC is also lower (see Table XIII). Additionally, in this geometry, the H_0 tension with Planck and local (SH0ES) data for \mathbf{D}_1 and \mathbf{D}_3 is substantially reduced.

In contrast, in the flat and open geometries, the differences are less pronounced, and the BIC criterion generally favors the simpler Λ CDM model (see Tables IX and XI).

Therefore, the R- Λ CDM model, particularly in the closed geometry, represents a more suitable option for alleviating the H_0 tension and warrants further investigation, whereas the flat and open models do not demonstrate a definitive advantage given the current data.

In conclusion, although the R- Λ CDM model does not fully resolve the H_0 tension, it offers significant improvements over the standard model, particularly in alleviating this discrepancy. Furthermore, the introduction of the ϵ parameter as a manifestation of matter–geometry interaction opens promising avenues for exploring extended physical scenarios.

Notably, ϵ tends to deviate from zero in the absence of full CMB data, potentially indicating physics beyond the standard model or underlying systematics in the observations.

Future progress in this field will strongly depend on the availability of more precise and comprehensive observational data. Recent and upcoming missions, such as *Euclid*, the *Nancy Grace Roman Space Telescope*, and next-generation CMB experiments including ACT and CMB-S4, are expected to play a pivotal role in tightening cosmological parameter constraints. In parallel, theoretical efforts to develop generalized gravity models, such as $f(R)$, $f(T)$, Horndeski theories, and interacting dark sector scenarios, must be pursued vigorously to take meaningful steps toward resolving current tensions and deepening our understanding of the universe.

Appendix A: Statistical Estimator for Quantifying Tension Between Datasets

A practical approach for evaluating potential statistical inconsistencies between two independent datasets, denoted as D_i and D_j , is to compare the marginalized one-dimensional posterior distributions of a given cosmological parameter α . To quantify such a discrepancy, a statistical estimator was proposed by [128], which computes the tension in terms of the number of standard deviations separating the parameter means. The estimator is defined as

$$N_\alpha = \frac{|\mu_{D_i} - \mu_{D_j}|}{\sqrt{\sigma_{D_i}^2 + \sigma_{D_j}^2}}, \quad (\text{A1})$$

where μ_{D_i} and μ_{D_j} represent the mean values of the parameter estimates obtained from the posterior distributions corresponding to datasets D_i and D_j , respectively, and σ_{D_i} and σ_{D_j} are the associated standard deviations. This method is widely used due to its simplicity, and we have also employed it to calculate and assess the discrepancies in cosmological parameters between different datasets.

-
- [1] Adam G et al. Riess. Observational evidence from supernovae for an accelerating universe and a cosmological constant. *Astron. J.*, 116(3):1009, 1998.
 - [2] Saul et al. Perlmutter. Measurements of ω and λ from 42 high-redshift supernovae. *Astrophys. J.*, 517(2):565, 1999.
 - [3] David N et al. Spergel. First-year wilkinson microwave anisotropy probe (wmap)* observations: determination of cosmological parameters. *Astrophys. J. Suppl. Ser.*, 148(1):175, 2003.
 - [4] P. James E. Peebles and Bharat Ratra. The cosmological constant and dark energy. *Rev. Mod. Phys.*, 75(2):559, 2003.
 - [5] Anatoly Pavlov, Shawn Westmoreland, Khaled Saaïdi, and Bharat Ratra. Nonflat time-variable dark energy cosmology. *Phys. Rev. D*, 88(12):123513, 2013.
 - [6] Shahnawaz A. Adil, Upala Mukhopadhyay, Anjan A. Sen, and Sunny Vagnozzi. Dark energy in light of the early jwst observations: case for a negative cosmological constant? *Journal of Cosmology and Astroparticle Physics*, 2023(10):072, 2023.
 - [7] Luis A. Escamilla, William Giarè, Eleonora Di Valentino, Rafael C. Nunes, and Sunny Vagnozzi. The state of the dark energy equation of state circa 2023. *Journal of Cosmology and Astroparticle Physics*, 2024(05):091, 2024.
 - [8] M. Vincenzi and et al. The dark energy survey supernova program: Cosmological analysis and systematic uncertainties. *The Astrophysical Journal*, 975(1):86, 2024.
 - [9] Alexei A. Starobinsky. A New Type of Isotropic Cosmological Models Without Singularity. *Phys. Lett. B*, 91:99–102, 1980.
 - [10] Alan H. Guth. The Inflationary Universe: A Possible Solution to the Horizon and Flatness Problems. *Phys. Rev.*, D23:347–356, 1981.
 - [11] Andreas Albrecht and Paul J. Steinhardt. Cosmology for Grand Unified Theories with Radiatively Induced Symmetry Breaking. *Phys. Rev. Lett.*, 48, 1982.
 - [12] Andrei D. Linde. A New Inflationary Universe Scenario: A Possible Solution of the Horizon, Flatness, Homogeneity, Isotropy and Primordial Monopole Problems. *Phys. Lett. B*, 108:389–393, 1982.
 - [13] Andrei D. Linde. Chaotic Inflation. *Phys. Lett. B*, 129:177–181, 1983.
 - [14] Michal Spalinski. On Power law inflation in DBI models. *JCAP*, 0705:017, 2007.
 - [15] Dennis Bessada, William H. Kinney, and Konstantinos Tzirakis. Inflationary potentials in DBI models. *JCAP*, 0909:031, 2009.
 - [16] N. Nazavari, A. Mohammadi, Z. Ossoulïan, and Kh. Saaïdi. Intermediate inflation driven by DBI scalar field. *Phys. Rev.*, D93(12):123504, 2016.
 - [17] Roonak Amani, Kazem Rezazadeh, Asrin Abdolmaleki, and Kayoomars Karami. Resurrecting the Power-law, Intermediate, and Logamediate Inflations in the DBI Scenario with Constant Sound Speed. *Astrophys. J.*, 853(2):188, 2018.
 - [18] Tayeb Golanbari, Abolhassan Mohammadi, and Khaled Saaïdi. Observational constraints on DBI constant-roll inflation. *Phys. Dark Univ.*, 27:100456, 2020.
 - [19] Arjun Berera. Warm inflation. *Physical Review Letters*, 75(18):3218, 1995.
 - [20] Arjun Berera. Warm inflation in the adiabatic regime—a model, an existence proof for inflationary dynamics in quantum field theory. *Nuclear Physics B*, 585(3):666–714, 2000.
 - [21] Mar Bastero-Gil and Arjun Berera. Determining the regimes of cold and warm inflation in the SUSY hybrid model. *Phys. Rev.*, D71:063515, 2005.
 - [22] João G. Rosa and Luís B. Ventura. Warm Little Inflaton becomes Cold Dark Matter. *Phys. Rev. Lett.*, 122(16):161301, 2019.
 - [23] Mar Bastero-Gil, Arjun Berera, Rudnei O. Ramos, and João G. Rosa. Towards a reliable effective field theory of inflation. 7 2019.
 - [24] K. Sayar, A. Mohammadi, L. Akhtari, and Kh. Saaïdi. Hamilton-Jacobi formalism to warm inflationary scenario. *Phys. Rev.*, D95(2):023501, 2017.
 - [25] L. Akhtari, A. Mohammadi, K. Sayar, and Kh. Saaïdi. Viscous warm inflation: Hamilton–Jacobi formalism. *Astropart. Phys.*, 90:28–36, 2017.
 - [26] Haidar Sheikahmadi, Abolhassan Mohammadi, Ali Aghamohammadi, Tiberiu Harko, Ramón Herrera, Christian Corda, Amare Abebe, and Khaled Saaïdi. Constraining chameleon field driven warm inflation with Planck 2018 data. *Eur. Phys. J.*, C79(12):1038, 2019.
 - [27] Mar Bastero-Gil, Sukannya Bhattacharya, Koushik Dutta, and Mayukh Raj Gangopadhyay. Constraining Warm Inflation with CMB data. *JCAP*, 02:054, 2018.
 - [28] Hayato Motohashi, Alexei A. Starobinsky, and Jun’ichi Yokoyama. Inflation with a constant rate of roll. *JCAP*, 1509:018, 2015.
 - [29] S. D. Odintsov, V. K. Oikonomou, and L. Sebastiani. Unification of Constant-roll Inflation and Dark Energy with Logarithmic R^2 -corrected and Exponential $F(R)$ Gravity. *Nucl. Phys.*, B923:608–632, 2017.
 - [30] V. K. Oikonomou. Reheating in Constant-roll $F(R)$ Gravity. *Mod. Phys. Lett.*, A32(33):1750172, 2017.
 - [31] Abolhassan Mohammadi, Tayeb Golanbari, and Khaled Saaïdi. Beta-function formalism for k-essence constant-roll inflation. *Phys. Dark Univ.*, 28:100505, 2020.
 - [32] Abolhassan Mohammadi, Tayeb Golanbari, Salah Nasri, and Khaled Saaïdi. Constant-roll brane inflation. *Phys. Rev. D*, 101:123537, 2020.
 - [33] Abolhassan Mohammadi. Constant-roll inflation driven by holographic dark energy. *Phys. Dark Univ.*, 36:101055, 2022.

- [34] Yogesh, Abolhassan Mohammadi, Qiang Wu, and Tao Zhu. Starobinsky like inflation and EGB Gravity in the light of ACT. 5 2025.
- [35] Abolhassan Mohammadi, Yogesh, and Anzhong Wang. Power Law Plateau Inflation and Primary Gravitational Waves in the light of ACT. 7 2025.
- [36] Antonio De Felice and Shinji Tsujikawa. $f(R)$ theories. *Living Rev. Rel.*, 13:3, 2010.
- [37] Thomas P. Sotiriou and Valerio Faraoni. $f(R)$ Theories Of Gravity. *Rev. Mod. Phys.*, 82:451–497, 2010.
- [38] Shin’ichi Nojiri and Sergei D. Odintsov. Unified cosmic history in modified gravity: from $f(r)$ theory to lorentz non-invariant models. *Phys. Rep.*, 505(2-4):59–144, 2011.
- [39] Gabriel R. Bengochea and Rafael Ferraro. Dark torsion as the cosmic speed-up. *Phys. Rev. D*, 79:124019, 2009.
- [40] Puxun Wu and Hong Wei Yu. Observational constraints on $f(T)$ theory. *Phys. Lett. B*, 693:415–420, 2010.
- [41] Ratbay Myrzakulov. Accelerating universe from $F(T)$ gravity. *Eur. Phys. J. C*, 71:1752, 2011.
- [42] Tiberiu Harko, Francisco S. N. Lobo, Shin’ichi Nojiri, and Sergei D. Odintsov. $f(r, t)$ gravity. *Phys. Rev. D*, 84(2):024020, 2011.
- [43] G. A. Carvalho, R. V. Lobato, P. H. R. S. Moraes, José D. V. Arbañil, R. M. Marinho, E. Otoniel, and M. Malheiro. Stellar equilibrium configurations of white dwarfs in the $f(R, T)$ gravity. *Eur. Phys. J. C*, 77(12):871, 2017.
- [44] Abolhassan Mohammadi and Fardin Kheirandish. Exploring new subclass of k -inflation: Tachyon inflation in $R+\eta T$ gravity model. *Phys. Dark Univ.*, 42:101362, 2023.
- [45] Z. Ossoulia, Kh. Saaidi, S. Taghavi, and T. Golanbari. Inflation in $f(R, T)$ gravity with observational constraints. 1 2023.
- [46] S. Taghavi, Kh. Saaidi, Z. Ossoulia, and T. Golanbari. Holographic inflation in $f(R, T)$ gravity and observational constraints. 1 2023.
- [47] Baojiu Li, John D. Barrow, and David F. Mota. The Cosmology of Modified Gauss-Bonnet Gravity. *Phys. Rev. D*, 76:044027, 2007.
- [48] Stephen C. Davis. Solar system constraints on $f(G)$ dark energy. 9 2007.
- [49] Yogesh and Abolhassan Mohammadi. Nonstandard Thermal History and Formation of Primordial Black Holes and SIGWs in Einstein–Gauss–Bonnet Gravity. *Astrophys. J.*, 986(1):35, 2025.
- [50] C. Brans and R. H. Dicke. Mach’s principle and a relativistic theory of gravitation. *Phys. Rev.*, 124:925–935, 1961.
- [51] S. Carloni, S. Capozziello, J. A. Leach, and P. K. S. Dunsby. Cosmological dynamics of scalar-tensor gravity. *Class. Quant. Grav.*, 25:035008, 2008.
- [52] Abolhassan Mohammadi, Tayeb Golanbari, Jamil Enayati, Shahram Jalalzadeh, Salah Nasri, and Khaled Saaidi. Swampland criteria and reheating predictions in scalar–tensor inflation. *Int. J. Mod. Phys. D*, 31(10):2250079, 2022.
- [53] Roy Maartens and Kazuya Koyama. Brane-World Gravity. *Living Rev. Rel.*, 13:5, 2010.
- [54] Ahmad Borzou, Hamid Reza Sepangi, Shahab Shahidi, and Raziieh Yousefi. Brane $f(R)$ gravity. *EPL*, 88(2):29001, 2009.
- [55] Abolhassan Mohammadi, Tayeb Golanbari, Salah Nasri, and Khaled Saaidi. Brane inflation: Swampland criteria, TCC, and reheating predictions. *Astropart. Phys.*, 142:102734, 2022.
- [56] B. Afshar, H. Moradpour, and H. Shabani. Slow-roll inflation and reheating in rastall theory. *Physics of the Dark Universe*, 42:101357, 2023.
- [57] Mustafa Salti. Propagation of axial gravitational waves in rastall gravity. *Physics of the Dark Universe*, 30:100630, 2020.
- [58] Rabia Saleem and Shahnila. Cosmological evolution via interacting/non-interacting holographic dark energy model for curved flrw space–time in rastall gravity. *Physics of the Dark Universe*, 32:100808, 2021.
- [59] N. Nazavari, Kh. Saaidi, and Abolhassan Mohammadi. Wormhole solution in modified teleparallel-Rastall gravity and energy conditions. *Gen. Rel. Grav.*, 55(3):45, 2023.
- [60] Nabila et al. Aghanim. Planck 2018 results-vi. cosmological parameters. *Astron. Astrophys.*, 641:A6, 2020.
- [61] P. A. R. et al. Ade. Planck 2013 results. xvi. cosmological parameters. *Astron. Astrophys.*, 571:A16, 2014.
- [62] P. A. R. et al. Ade. Planck 2015 results. xiii. cosmological parameters. *Astron. Astrophys.*, 594:A13, 2016.
- [63] Adam G. Riess, Stefano Casertano, Wenlong Yuan, Lucas M. Macri, and Dan Scolnic. Large magellanic cloud cepheid standards provide a 1% foundation for the determination of the hubble constant and stronger evidence for physics beyond Λ cdm. *Astrophys. J.*, 876(1):85, 2019.
- [64] Adam G. Riess, Stefano Casertano, Wenlong Yuan, J. Bradley Bowers, Lucas Macri, Joel C. Zinn, and Dan Scolnic. Cosmic distances calibrated to 1% precision with gaia edr3 parallaxes and hubble space telescope photometry of 75 milky way cepheids confirm tension with Λ cdm. *Astrophys. J. Lett.*, 908(1):L6, 2021.
- [65] Salvatore Capozziello, Giuseppe Sarracino, and Alessandro D.A.M. Spallicci. Questioning the h_0 tension via the look-back time. *Physics of the Dark Universe*, 40:101201, 2023.
- [66] Licia Verde, Tommaso Treu, and Adam G. Riess. Tensions between the early and late universe. *Nature Astron.*, 3(10):891–895, 2019.
- [67] et al. Di Valentino. Snowmass2021-letter of interest cosmology intertwined ii: The hubble constant tension. *Astropart. Phys.*, 131:102605, 2021.
- [68] Kenneth C. et al. Wong. Holicow–xiii. a 2.4 per cent measurement of h_0 from lensed quasars: 5.3 σ tension between early-and late-universe probes. *Mon. Not. Roy. Astron. Soc.*, 498(1):1420–1439, 2020.
- [69] Philipp Denzel, Jonathan P. Coles, Prasenjit Saha, and Liliya L. R. Williams. The hubble constant from eight time-delay galaxy lenses. *Mon. Not. Roy. Astron. Soc.*, 501(1):784–801, 2021.
- [70] Wendy L. et al. Freedman. The carnegie-chicago hubble program. viii. an independent determination of the hubble constant based on the tip of the red giant branch. *Astrophys. J.*, 882(1):34, 2019.
- [71] Wendy L. et al. Freedman. Calibration of the tip of the red giant branch. *Astrophys. J.*, 891(1):57, 2020.

- [72] Eric J. Baxter and Blake D. Sherwin. Determining the hubble constant without the sound horizon scale: measurements from cmb lensing. *Mon. Not. Roy. Astron. Soc.*, 501(2):1823–1835, 2021.
- [73] D. W. Pesce, J. A. Braatz, M. J. Reid, A. G. Riess, D. Scolnic, J. J. Condon, F. Gao, C. Henkel, C. M. V. Impellizzeri, C. Y. Kuo, and K. Y. Lo. The megamaser cosmology project. xiii. combined hubble constant constraints. *Astrophys. J. Lett.*, 891(1):L1, 2020.
- [74] Caroline D. et al. Huang. Hubble space telescope observations of mira variables in the sn ia host ngc 1559: An alternative candle to measure the hubble constant. *Astrophys. J.*, 889(1):5, 2020.
- [75] ACT Collaboration et al. The atacama cosmology telescope: Dr6 constraints on extended cosmological models. *arXiv*, 2503.14454, 2025.
- [76] ACT Collaboration et al. Early dark energy and the hubble tension: Constraints from act dr6 and desi dr2. *arXiv*, 2025. arXiv:2505.08051.
- [77] Guillermo Ballesteros, Alessio Notari, and Fabrizio Rompineve. The h_0 tension: δg_n vs. δn_{eff} . *J. Cosmol. Astropart. Phys.*, 2020(11):024, 2020.
- [78] Miguel Zumalacarregui. Gravity in the era of equality: Towards solutions to the hubble problem without fine-tuned initial conditions. *Phys. Rev. D*, 102(2):023523, 2020.
- [79] Sergei D. Odintsov, Diego Sáez-Chillón Gómez, and German S. Sharov. Analyzing the h_0 tension in $f(r)$ gravity models. *Nucl. Phys. B*, 966:115377, 2021.
- [80] Qing-Guo Huang and Ke Wang. How the dark energy can reconcile *Planck* with local determination of the hubble constant. *arXiv preprint*, 2016.
- [81] Francesco D’Eramo, Ricardo Z. Ferreira, Alessio Notari, and José Luis Bernal. Hot axions and the h_0 tension. *J. Cosmol. Astropart. Phys.*, 2018(11):014, 2018.
- [82] Eleonora Di Valentino, Alessandro Melchiorri, and Olga Mena. Can interacting dark energy solve the h_0 tension? *Phys. Rev. D*, 96(4):043503, 2017.
- [83] Albert Petrov, Jose Roberto Nascimento, and Paulo Porfirio. *Introduction to Modified Gravity*. SpringerBriefs in Physics. Springer, 7 2020.
- [84] Francisco S. N. Lobo and Tiberiu Harko. Curvature–matter couplings in modified gravity: From linear models to conformally invariant theories. *Int. J. Mod. Phys. D*, 31(11):2240010, 2022.
- [85] Omer Farooq, Foram Ranjeet Madiyar, Sara Crandall, and Bharat Ratra. Hubble parameter measurement constraints on the redshift of the deceleration–acceleration transition, dynamical dark energy, and space curvature. *Astrophys. J.*, 835(1):26, 2017.
- [86] Paolo Serra, Asantha Cooray, Daniel E. Holz, Alessandro Melchiorri, Stefania Pandolfi, and Devdeep Sarkar. No evidence for dark energy dynamics from a global analysis of cosmological data. *Phys. Rev. D*, 80:121302, 2009.
- [87] David Camarena and Valerio Marra. Impact of the cosmic variance on h_0 on cosmological analyses. *Phys. Rev. D*, 98(2):023537, 2018.
- [88] Lu Chen, Qing-Guo Huang, and Ke Wang. Distance priors from planck final release. *JCAP*, 02:028, 2019.
- [89] Savvas Nesseris, George Pantazis, and Leandros Perivolaropoulos. Tension and constraints on modified gravity parametrizations of $g_{\text{eff}}(z)$ from growth rate and planck data. *Phys. Rev. D*, 96(2):023542, 2017.
- [90] Antony Lewis and Sarah Bridle. Cosmological parameters from cmb and other data: A monte carlo approach. *Physical Review D*, 66(10):103511, 2002.
- [91] Paolo Serra, Asantha Cooray, Daniel E. Holz, Alessandro Melchiorri, Stefania Pandolfi, and Devdeep Sarkar. No evidence for dark energy dynamics from a global analysis of cosmological data. *Phys. Rev. D*, 80(12):121302, 2009.
- [92] Zhang-Jin Zhang, Xiao-Min Wang, and Grainne M McAlonan. Neural acupuncture unit: a new concept for interpreting effects and mechanisms of acupuncture. *Evidence-Based Complementary and Alternative Medicine*, 2012(1):429412, 2012.
- [93] Chris et al. Blake. The wigglez dark energy survey: Joint measurements of the expansion and growth history at $z \lesssim 1$. *Mon. Not. Roy. Astron. Soc.*, 425(1):405–414, 2012.
- [94] Joshua D. Simon, Alberto D. Bolatto, Adam Leroy, Leo Blitz, and Elinor L. Gates. High-resolution measurements of the halos of four dark matter-dominated galaxies: deviations from a universal density profile. *Astrophys. J.*, 621(2):757, 2005.
- [95] GM Monirul Alam, Khorshed Alam, and Shahbaz Mushtaq. Climate change perceptions and local adaptation strategies of hazard-prone rural households in bangladesh. *Climate Risk Management*, 17:52–63, 2017.
- [96] Michele et al. Moresco. Improved constraints on the expansion rate of the universe up to $z \sim 1.1$ from the spectroscopic evolution of cosmic chronometers. *J. Cosmol. Astropart. Phys.*, 2012(08):006, 2012.
- [97] Daniel Stern, Raul Jimenez, Licia Verde, Marc Kamionkowski, and S. Adam Stanford. Cosmic chronometers: constraining the equation of state of dark energy. i: $H(z)$ measurements. *J. Cosmol. Astropart. Phys.*, 2010(02):008, 2010.
- [98] Michele Moresco. Raising the bar: new constraints on the hubble parameter with cosmic chronometers at $z \sim 2$. *Monthly Notices of the Royal Astronomical Society: Letters*, 450(1):L16–L20, 2015.
- [99] Michele et al. Moresco. A 6% measurement of the hubble parameter at $z \sim 0.45$: direct evidence of the epoch of cosmic re-acceleration. *Journal of Cosmology and Astroparticle Physics*, 2016(05):014, 2016.
- [100] Guangtun Ben et al. Zhu. Near-ultraviolet spectroscopy of star-forming galaxies from eboss: signatures of ubiquitous galactic-scale outflows. *The Astrophysical Journal*, 815(1):48, 2015.
- [101] et al. Font-Ribera. Quasar-lyman α forest cross-correlation from boss dr11: Baryon acoustic oscillations. *Journal of Cosmology and Astroparticle Physics*, 2014(05):027, 2014.
- [102] M. Malekjani, S. Basilakos, A. Mehrabi, Z. Davari, and M. Rezaei. Agegraphic dark energy: growth index and cosmological implications. *Monthly Notices of the Royal Astronomical Society*, 464(1):1192–1201, 2016.
- [103] Wayne Hu and Naoshi Sugiyama. Small-scale cosmological perturbations: an analytic approach. *The Astrophysical*

Journal, 471(2):1996, 542, 1996.

- [104] Dragan Huterer, Daniel L. Shafer, Daniel M. Scolnic, and Fabian Schmidt. Testing λ cdm at the lowest redshifts with sn ia and galaxy velocities. *J. Cosmol. Astropart. Phys.*, 2017(05):015, 2017.
- [105] Michael J. Hudson and Stephen J. Turnbull. The growth rate of cosmic structure from peculiar velocities at low and high redshifts. *Astrophys. J. Lett.*, 751(2):L30, 2012.
- [106] Stephen J. Turnbull, Michael J. Hudson, Hume A. Feldman, Malcolm Hicken, Robert P. Kirshner, and Richard Watkins. Cosmic flows in the nearby universe from type ia supernovae. *Mon. Not. Roy. Astron. Soc.*, 420(1):447–454, 2012.
- [107] Marc Davis, Adi Nusser, Karen L Masters, Christopher Springob, John P Huchra, and Gerard Lemson. Local gravity versus local velocity: solutions for β and non-linear bias. *Monthly Notices of the Royal Astronomical Society*, 413(4):2906–2922, 2011.
- [108] Martin Feix, Adi Nusser, and Enzo Branchini. Growth rate of cosmological perturbations at $z=0.1$ from a new observational test. *Physical Review Letters*, 115(1):011301, 2015.
- [109] Cullan Howlett, Ashley J Ross, Lado Samushia, Will J Percival, and Marc Manera. The clustering of the sdss main galaxy sample–ii. mock galaxy catalogues and a measurement of the growth of structure from redshift space distortions at $z=0.15$. *Monthly Notices of the Royal Astronomical Society*, 449(1):848–866, 2015.
- [110] Yong-Seon Song and Will J Percival. Reconstructing the history of structure formation using redshift distortions. *Journal of Cosmology and Astroparticle Physics*, 2009(10):004, 2009.
- [111] Chris et al. Blake. Galaxy and mass assembly (gama): improved cosmic growth measurements using multiple tracers of large-scale structure. *Monthly Notices of the Royal Astronomical Society*, 436(4):3089–3105, 2013.
- [112] Lado Samushia, Will J Percival, and Alvis Raccanelli. Interpreting large-scale redshift-space distortion measurements. *Monthly Notices of the Royal Astronomical Society*, 420(3):2102–2119, 2012.
- [113] Ariel G et al. Sánchez. The clustering of galaxies in the sdss-iii baryon oscillation spectroscopic survey: cosmological implications of the full shape of the clustering wedges in the data release 10 and 11 galaxy samples. *Monthly Notices of the Royal Astronomical Society*, 440(3):2692–2713, 2014.
- [114] Chia-Hsun et al. Chuang. The clustering of galaxies in the sdss-iii baryon oscillation spectroscopic survey: single-probe measurements from cmass anisotropic galaxy clustering. *Monthly Notices of the Royal Astronomical Society*, 461(4):3781–3793, 2016.
- [115] Shadab et al. Alam. The clustering of galaxies in the completed sdss-iii baryon oscillation spectroscopic survey: cosmological analysis of the dr12 galaxy sample. *Monthly Notices of the Royal Astronomical Society*, 470(3):2617–2652, 2017.
- [116] Teppei et al. Okumura. The subaru fmos galaxy redshift survey (fastsound). iv. new constraint on gravity theory from redshift space distortions at $z=1.4$. *Publications of the Astronomical Society of Japan*, 68(3):38, 2016.
- [117] LR Abramo, Ronaldo Cardoso Batista, L Liberato, and Rogério Rosenfeld. Physical approximations for the nonlinear evolution of perturbations in inhomogeneous dark energy scenarios. *Physical Review D*, 79(2):2009, 023516, 2009.
- [118] Salvatore Capozziello, Ruth Lazkoz, and Vincenzo Salzano. Comprehensive cosmographic analysis by markov chain method. *Physical Review D—Particles, Fields, Gravitation, and Cosmology*, 84(12):2011, 124061, 2011.
- [119] Robert E Kass and Adrian E Raftery. Bayes factors. *Journal of the american statistical association*, 90(430):1995, 773–795, 1995.
- [120] David J Spiegelhalter, Nicola G Best, Bradley P Carlin, and Angelika Van Der Linde. Bayesian measures of model complexity and fit. *Journal of the royal statistical society: Series b (statistical methodology)*, 64(4):2002, 583–639, 2002.
- [121] HAL Whitehead. Selection of models of lagged identification rates and lagged association rates using aic and qaic. *Communications in Statistics-Simulation and Computation*, 36(6):2007, 1233–1246, 2007.
- [122] Andrew R Liddle. Information criteria for astrophysical model selection. *Monthly Notices of the Royal Astronomical Society: Letters*, 377(1):2007, L74–L78, 2007.
- [123] Mehdi Rezaei and Mohammad Malekjani. Comparison between different methods of model selection in cosmology. *The European Physical Journal Plus*, 136(2):2021, 219, 2021.
- [124] Simone Aiola, Erminia Calabrese, Loïc Maurin, and et al. The atacama cosmology telescope: Dr4 maps and cosmological parameters. *Journal of Cosmology and Astroparticle Physics*, 2020(12):2020, 047, 2020.
- [125] David Qu, J. Colin Hill, Steve K. Choi, and et al. The atacama cosmology telescope: Dr6 cosmological parameters. *Journal of Cosmology and Astroparticle Physics*, 2023(10):2023, 012, 2023.
- [126] Planck Collaboration, N. Aghanim, et al. Planck 2018 results. vi. cosmological parameters. *Astronomy & Astrophysics*, 641:2020, A6, 2020.
- [127] Adam G. Riess, Stefano Casertano, Wenlong Yuan, and et al. A comprehensive measurement of the local value of the hubble constant with $1 \text{ km s}^{-1} \text{ mpc}^{-1}$ uncertainty from the hubble space telescope and the sh0es team. *The Astrophysical Journal Letters*, 934(1):2022, L7, 2022.
- [128] Tensions in cosmology: A discussion of statistical tools to determine inconsistencies. *Physics Letters B*, 855:2024, 138844, 2024.